Mechanical Behaviour of Concrete under Torsional Loading at Transient, Hightemperature Conditions

Thelandersson, Sven

1974

LUND INSTITUTE OF TECHNOLOGY · LUND · SWEDEN · 1974
DIVISION OF STRUCTURAL MECHANICS AND CONCRETE CONSTRUCTION · BULLETIN 46

SVEN THELANDERSSON

MECHANICAL BEHAVIOR OF CONCRETE UNDER TORSIONAL LOADING AT TRANSIENT, HIGH-TEMPERATURE CONDITIONS

LUND INSTITUTE OF TECHNOLOGY LUND SWEDEN 1974
DIVISION OF STRUCTURAL MECHANICS AND CONCRETE CONSTRUCTION

MECHANICAL BEHAVIOUR OF CONCRETE UNDER TORSIONAL LOADING AT TRANSIENT, HIGH-TEMPERATURE CONDITIONS

Sven Thelandersson

LUND, NOV 1974

Contents

Abstract

The purpose of this paper is to study the deformations under load in concrete at transient high-temperature conditions. The study is made on the basis of tests of plain concrete in pure torsion, which makes it possible to study the deformations under changing temperature without simultaneous thermal dilatation being included. The test series comprises four different types of tests, viz. torque vs. twist at constant temperature, creep at constant load and temperature, heating to failure under constant load and heating to a maximum temperature level under constant load.

It is shown that the deformations of stressed concrete under heating can not be predicted on the basis of tests performed at constant temperatures. The total deformation is described in terms of three components, instantaneous strain, constant temperature creep and transient strain, the latter occurring under load as a response to a temperature increase. The different components are formulated mathematically and employed in a theoretical analysis of stresses and deformations. The theory is used to analyse torsion tests on specimens with circular cross section and very good agreement is found for a wide range of loading and temperature conditions.

In a qualitative sense the theory developed may be used to predict deformations in compression and direct tension as well, and can thus be an important step towards a thorough understanding of the structural behaviour of reinforced and prestressed concrete under transient thermal exposure.

Acknowledgements

This paper is the final report from a research project sponsored by the Swedish Council of Building Research. The author wishes to thank the Council for this support.

Parts of the experimental investigation was made as two different graduate works, the one by Tommy Isaksson and Ingmar Ström and the other by Hans-Göran Jansson, Ulf Lagerström and Tommy Larsson.

The author wants to thank Professor Ove Pettersson for providing fruitful ideas and encouraging support. Thanks are also due to the whole staff of the Division of Structural Mechanics and Concrete Construction and in particular the persons listed below.
Leif Ljungquist manufactured the test rig.
Aldo Lindsjö built the furnace.
Karl Erik Bohlin made most of the specimens.
Kjell Andersson, Lennart Andersson and Sven-Ingvar Granemark assisted in the performance of the tests.
Ann Schollin made the drawings.
Lisbeth Henning and Eivor Nilsson typed the manuscript.

1. Introduction

In recent years, the mechanical behaviour of concrete at high temperatures has been the subject of an increasing interest. The use of concrete in nuclear reactor pressure vessels has initiated extensive research efforts as regards the properties of concrete in the range 0 - 200°C and in the structural fire protection field the development towards more functional design procedures has created a need for more detailed information about the effect of temperatures up to as high as 800°C on concrete.

Any attempt to analyse the structural behaviour of a reinforced or prestressed concrete member under thermal exposure and static load involves an estimate of stresses and deformations in the concrete and the steel. For steel the mechanical behaviour at high temperatures is rather well-known, see for instance /1/ and /2/, while an analysis of stresses and deformations in loaded, heated concrete is very difficult to make. This is due to the fact that a realistic constitutive equation for concrete under transient, high-temperature conditions has not yet been formulated. To achieve this end, further information is required about the deformation under load of concrete exposed to high temperatures.

For temperatures below 100°C a constitutive relationship has been put forward by Bazant /3/, based on a theory of the thermodynamical equilibrium of the diffusible load-bearing layers in the cement gel, taking into account temperature, humidity, age and type of load. Bazant's equation has been applied successfully for predicting creep at variable temperatures in the range 20 - 100°C /4/. This equation is of a very complicated nature and a simplified model has recently been presented by Fahmi et al. /5/. In an advanced computer program for structural analysis of reinforced concrete under fire exposure, Becker & Bresler /26/ have included the effect of concrete creep and shrinkage. The creep model, which is based on work by Mukaddam /12/, is correlated with creep data obtained at constant temperatures.

In /6/ the state of art as regards the deformation characteristics of concrete at high temperatures was accounted for, and the need for further research was discussed. It is obvious that predicting

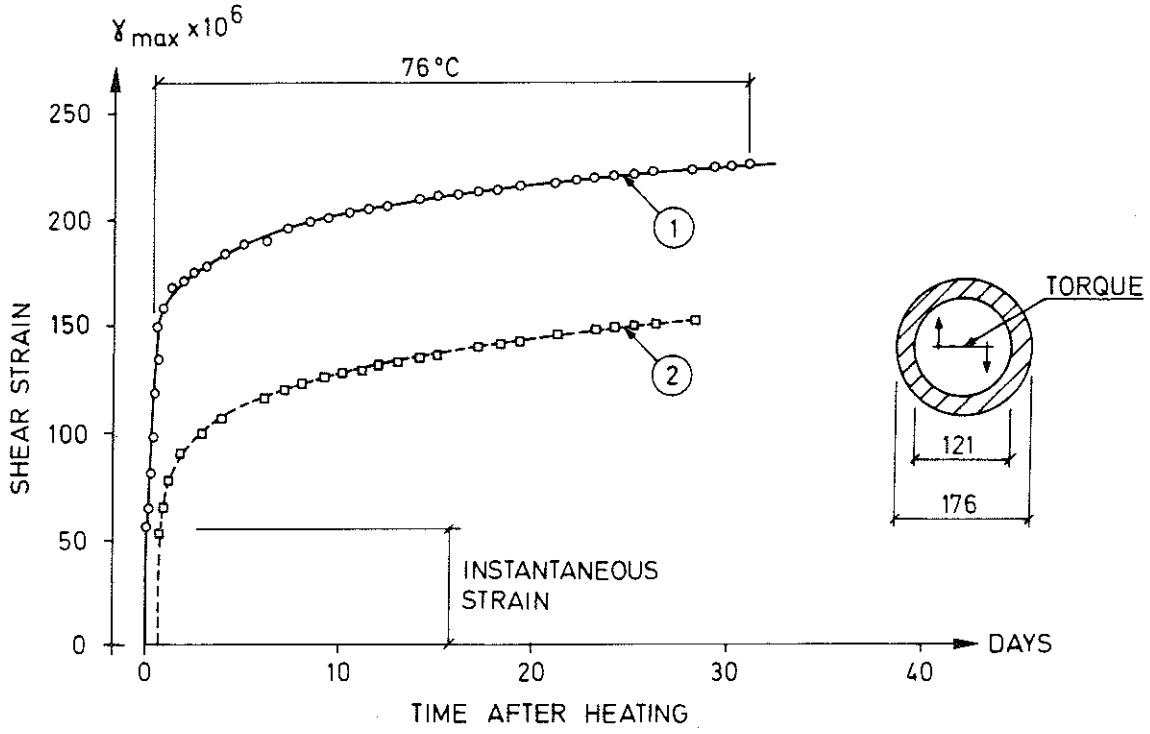

Figure 1. Strains of mortar specimens with torsional load applied just before (curve 1) and just after (curve 2) heating from 20°C to 76°C. Rate of heating: 5.1°C·h^{-1}. The load level corresponded to a maximum principal tensile stress of 0.67 MPa, 16 % of the cylinder-splitting strength. Age of heating: 40 days. Mix proportions: Cement/sand = 1/2, w/c = 0.45.

the deformations under load in heated concrete is a very difficult task. Compared with metal or ceramic materials, concrete exhibits a special feature, viz. that the deformations under transient conditions can not be predicted on the basis of tests made at constant temperatures. During heating of stressed concrete, considerable deformations develop which do not accur under stabilized temperature. This "transient deformation" is a very important component of the total deformation and can never be neglected.

The effect of changing temperature on the deformations at moderate temperatures has been studied by Hansen & Eriksson /7/ and Illston & Sanders /8/. In figure 1 is shown the results obtained in /8/ on mortar specimens under torsional loading. The figure gives the total shear strain in thinwalled tubular specimens heated from 20°C to 76°C, as a function of the time after the start of heating. The same constant torque was applied either before heating (curve 1) or just after heating (curve 2). The specimens were sealed and filled with water to avoid sorption creep during the test, and the difference between curve 1 and 2 can therefore be directly related to the temperature increase. In this paper, the deformation component defined by this difference will be termed transient deformation [1]. Illston & Sanders also found that the magnitude of the transient deformation was virtually the same whether the temperature increase was made in one single step or in several steps. The results in /8/ also indicate that the transient component is irrecoverable and occurs only under the first heating and not under cooling. The same behaviour was found in compression tests performed by Nishizawa & Okamura /9/.

Apart from the transient strain component, a model capable of predicting the deformation under load at variable, high temperatures must contain components for instantaneous elastic and inelastic strains, thermal dilatation and constant temperature creep.

The purpose of this paper is to study basic problems inherent in establishing such a model. Tests of concrete in torsion, designed for this purpose, will be accounted for. By studying torsion instead of compression the thermal expansion component can be avoided and

---

1) In /8/ is used the name transitional creep.

the response to load at variable temperatures can be directly measured. It is commonly accepted that the creep behaviour in torsion is qualitatively the same as that in compression /4, 10/.

The investigation is mainly aimed at studying deformations and stresses under conditions representative for fire exposure, which means that the rate of heating is relatively high and that only short periods of time are studied.

2. Experimental Procedure

2.1 Test Program

The tests were made in pure torsion on prismatic beams with two different cross sections, viz. circular, diameter 150 mm and square, 150 x 150 mm. The main part of the test program comprises circular specimens, which have a simple shear stress distribution. The disadvantage with the selected cross sections is that an undesirable extra variable, the stress gradient over the cross section, is introduced. This could have been avoided by using tubular instead of solid specimens, but this would have meant that ordinary concrete could not have been used. Besides that, the moisture migration conditions would be unrealistic in a thin-walled concrete tube.

The test series is divided into four main types of tests:

A. The specimen was heated to a certain temperature and then loaded to failure.
B. The specimen was heated to a certain temperature and then loaded, whereafter the creep was observed. After 3 hrs the load was removed, the recovery was observed during 15 min., and the specimen was then loaded to failure.
C. The specimen was loaded and then heated to failure at a certain rate of heating.
D. The specimen was loaded and then heated to a certain temperature, while the creep was observed. The load was removed 5 hrs after the temperature was reached, the recovery was observed during 15 min., and the specimen was then loaded to failure.

The load and furnace temperature histories in the four different cases are illustrated in figure 2.

The main parameters varied in the test series were

Temperature level (20 - 500°C)
Rate of heating (2, 4 and 8°C·min^{-1})
Load level (15, 30, 45 and 60 % of ultimate load at 20°C)

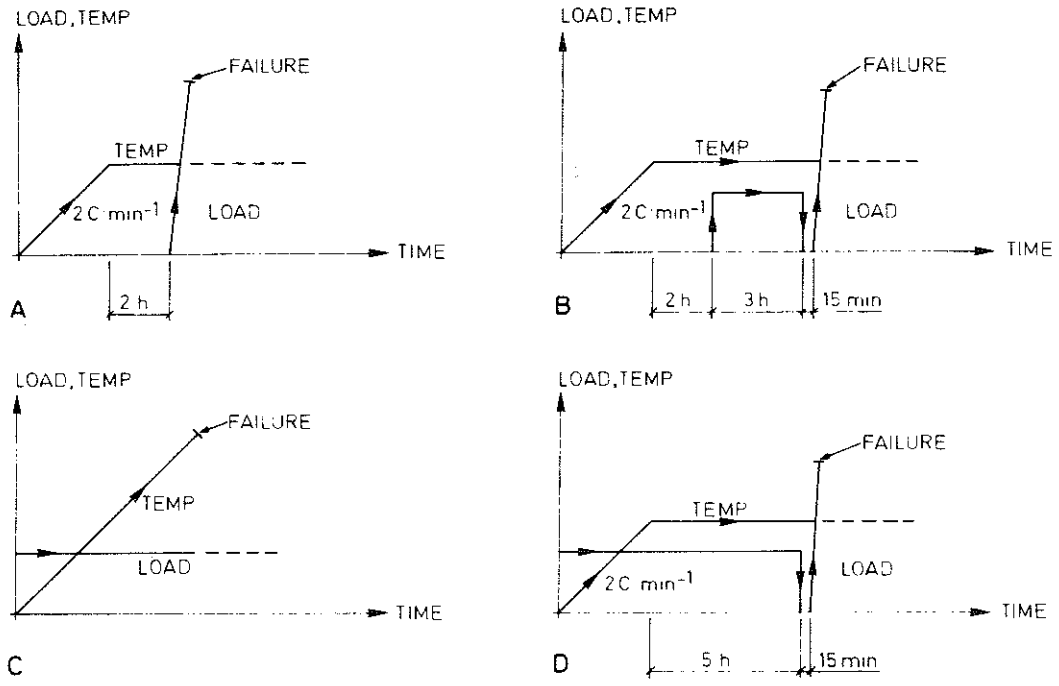

Figure 2. Load and temperature histories used in the four different types of tests.

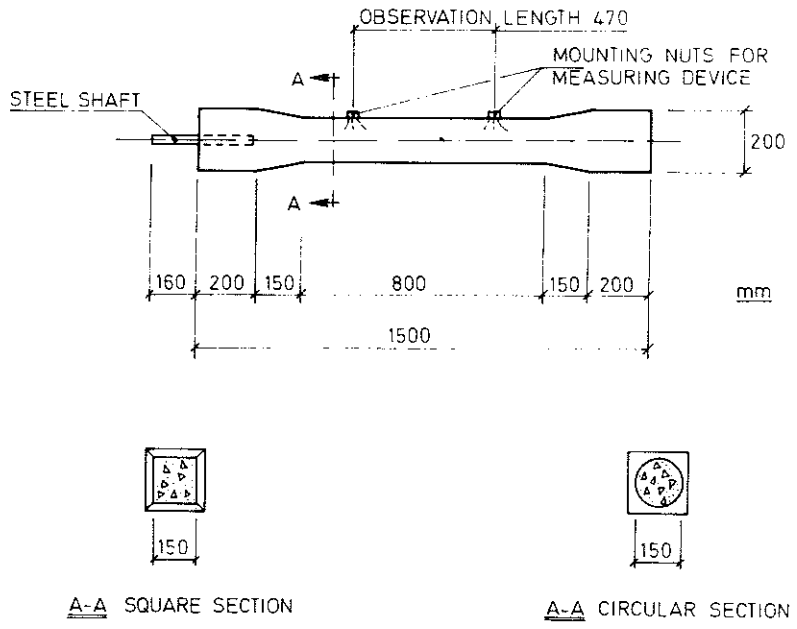

Figure 3. Dimensions of the test specimens.

The temperature in the A and B series was limited to 400°C. Upon heating to 500°C or above this level the specimens tended to fail in bending due to their own weight.

The test program is summarized in table 1, where reference is made to the four types of tests A - D. In the same table is given the cube strength(average of three 15 cm cubes) and the split-cylinder tensile strength (average of 6 cylinders, diameter 94 mm, length 190 mm) for the concretes used for respective specimens. The temperature indicated in table 1 is the desired temperature, in some cases the real measured temperature is slightly different. In the presentation of results the real measured values will be used. In the table is indicated the desired load level in % of the ultimate torque at ambient conditions, determined from the tests A1 - A6, as well as the actually measured values in Nm. The actually applied loads were by mistake somewhat (≈ 10 %) higher than the desired values in series B and D. This will not in any way affect the further treatment, however.

2.2 Specimens and Materials

The geometry of the test specimens is shown in figure 3. The twist measurements were made on a length of 470 mm in the middle part. The specimens were made thicker at the ends to avoid failure near the supports.

The specimens were cast vertically and vibrated with tube at several levels. The concrete was made from standard Portland Cement (Limhamn), sand ($\leq$ 8 mm) of glacial origin and macadam (8 - 12 mm) of quartzite (97 - 98 % quartz, 2 - 3 % feldspars). All specimens were made with the same mix proportions, in weight units:

Cement	1
Water	0.55
Sand	2.65
Macadam	2.00

The mix was designed to give a cube strength of 40 MPa at 28 days. As seen from table 1, the scatter between different batches is considerable (coefficient of variation 16 %) and the cube strength varies between 32.3 and 54 MPa. This scatter affects the validity of

TABLE 1. TEST PROGRAM

No	Temp	Rate of heating	Load	Load	Number of specimens	Cross section	Cube strength	Tensile strength	Ultimate torque
	°C	°C·min^{-1}	N·m	%			MPa	MPa	N·m
A1	20	-	-	-	2	C	54.0	4.19	2140
A2	20	-	-	-	2	S	54.0	4.19	3170
A3	20	-	-	-	2	C	46.3	3.88	1980
A4	20	-	-	-	2	S	46.3	3.88	2990
A5	20	-	-	-	2	C	53.7	4.16	2105
A6	20	-	-	-	2	S	53.7	4.16	3165
A7	100	2	-	-	1	C	42.5	3.83	1150
A8	100	2	-	-	1	C	32.2	3.02	990
A9	100	2	-	-	2	S	42.5	4.16	1835
A10	200	2	-	-	2	C	46.8	4.56	1835
A11	200	2	-	-	2	S	46.8	4.56	2630
A12	300	2	-	-	2	C	39.8	3.61	1250
A13	300	2	-	-	2	S	39.8	3.61	1280
A14	400	2	-	-	1	C	53.8	4.32	1550
A15	400	2	-	-	1	C	45.9	3.47	1340
A16	400	2	-	-	2	S	53.8	4.32	1835
B1	20	2	670	30	1	C	34.1	3.21	1370
B2	20	2	1120	60	1	C	34.1	3.21	-
B3	70	2	685	30	1	C	43.0	3.19	1420
B4	130	2	670	30	1	C	38.4	3.64	1270
B5	200	2	680	30	1	C	35.9	2.97	1540
B6	300	2	670	30	1	C	41.6	3.37	2460
B7	400	2	670	30	1	C	39.2	3.46	1200
B8	400	2	665	30	1	C	45.1	3.69	-
C1	-	2	603	30	1	C	32.3	2.74	-
C2	-	2	612	30	1	C	32.3	2.74	-
C3	-	2	954	30	1	S	32.3	2.74	-
C4	-	2	923	30	1	S	32.3	2.74	-
C5	-	2	1239	60	1	C	40.6	3.15	-
C6	-	2	1234	60	1	C	40.6	3.15	-
C7	-	4	357	15	1	C	51.2	3.89	-
C8	-	4	630	30	1	C	53.0	3.51	-
C9	-	4	917	45	1	C	49.0	3.57	-
C10	-	4	1232	60	1	C	49.6	3.88	-
C11	-	8	612	30	1	C	39.0	3.02	-
C12	-	8	612	30	1	C	39.0	3.02	-
C13	-	8	925	30	1	S	39.0	3.02	-
C14	-	8	911	30	1	S	39.0	3.02	-
C15	-	8	1230	60	1	C	37.5	2.80	-
C16	-	8	1230	60	1	C	37.5	2.80	-

C = Circular S = Square

TABLE 1, continued

No	Temp	Rate of heating	Load	Load	Number of specimens	Cross section	Cube strength	Tensile strength	Ultimate torque
	°C	°C·min^{-1}	N·m	%			MPa	MPa	N·m
D1	70	2	680	30	1	C	43.0	3.19	-
D2	130	2	690	30	1	C	38.4	3.64	1510
D3	200	2	335	15	1	C	53.8	3.72	1550
D4	200	2	660	30	1	C	35.9	2.97	1410
D5	200	2	1000	45	1	C	44.2	3.61	1420
D6	200	2	1350	60	1	C	44.2	3.61	1690
D7	300	2	670	30	1	C	45.1	3.69	2030
D8	400	2	670	30	1	C	39.2	3.46	935
D9	500	2	680	30	1	C	53.8	3.72	840

C = Circular S = Square

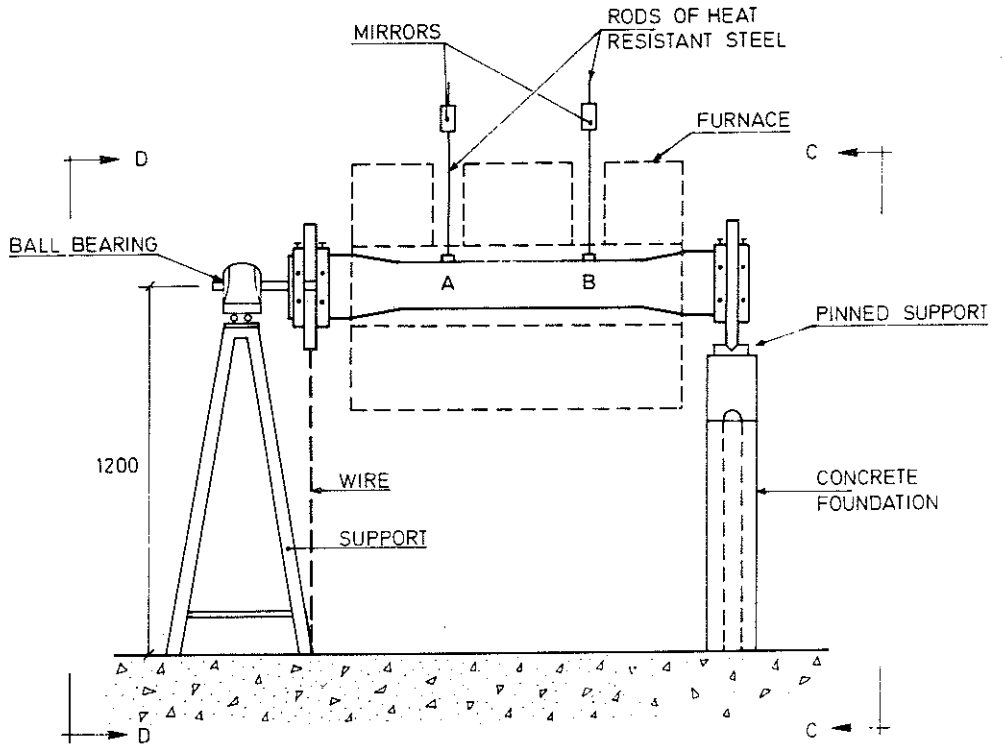

a)

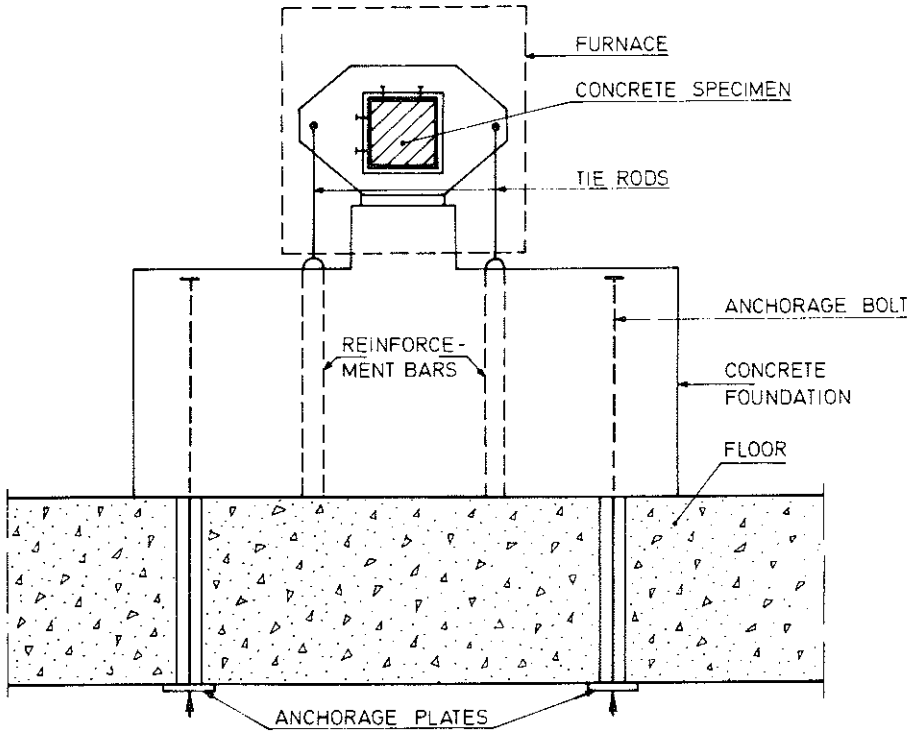

SECTION C-C

b)

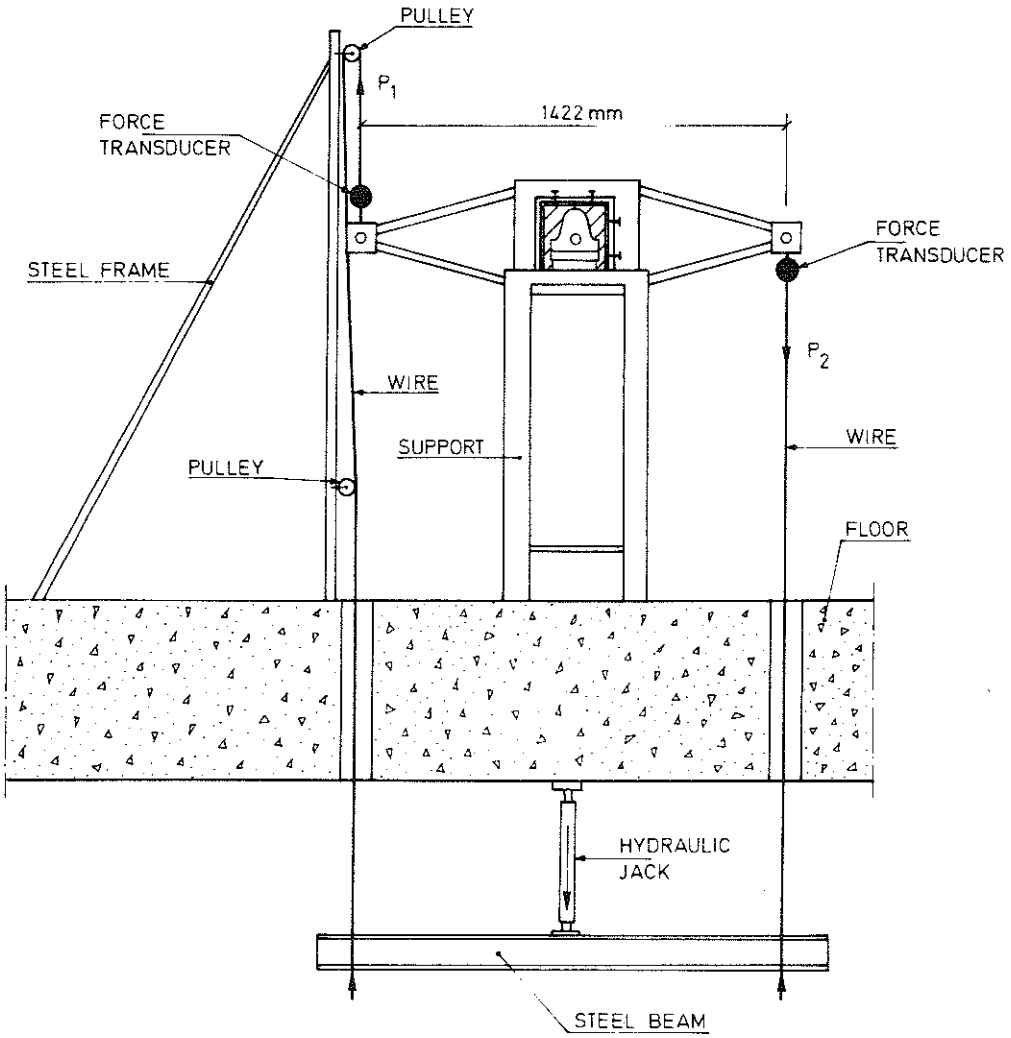

c)

Figure 4. Torsion test rig.
a) Side view
b) View of fixed end
c) View of load application.

comparisons between different tests, a fact which must be taken into account in the interpretation of the results.

The specimens were standard cured, i.e. 1 day in the mould, 5 days under wet sacking, and the rest of the time prior to testing at 28 days in climate chamber with 65 % RH, 20°C. At the time of testing the moisture content amounted to about 6 % in the core and 4 % near the surface.

2.3 Test Rig and Loading

The torsion test rig is shown in figure 4. The specimen is fixed against torsional rotation at one end (right hand side in figure 4a), and the torque is applied at the other end. At the fixed end angular displacements due to bending are allowed for but not horizontal displacements (pinned support). At the other end of the specimen a steel shaft coinciding with the central axis is cast in. The steel shaft rests on a ball bearing, which allows for rotations around the longitudinal axis as well as the horizontal axis perpendicular to the longitudinal direction. The ball bearing rests on cylindrical bearings, admitting horizontal displacements. The torsional moment is realized with a couple of forces P_1 and P_2 acting on cantilevers mounted on the specimen as shown in figure 4c. The forces P_1 and P_2 are produced by a hydraulic jack under the floor, and are transferred to the cantilevers with steel wires. The magnitudes of P_1 and P_2 are measured with force transducers (AB BOFORS, type KRG4, 0 - 1000 kp) placed between the wires and the cantilevers. The forces were continuously recorded on a 2-channel potentiometer pen-recorder (Servogor), with the precision ± 15 N. Due to friction in the pulleys P_1 was slightly smaller than P_2, the difference being about 10 %. In the test series B, C and D, where the load was held constant throughout the tests, the jack was replaced by water containers hanging in the wires.

In all the tests the load was applied in steps of 150 - 250 Nm each, the higher value for the rectangular specimens. The time interval between the steps was as a rule about 1 minute. In the test series B and D the loading to failure at the end of the test was made continuously at a rate of 250 - 300 Nm/min and no measurements of deformation were made.

2.4 Twist Measurements

The absolute angle of twist was measured at two points on the specimen, A and B in figure 4a, situated at a distance of 470 mm from each other. The difference between these two angles divided by the distance gives the desired quantity ϕ (twist/unit length). Vertical rods of heat resistant steel were attached at the points A and B and led through apertures out of the furnace, where mirrors were mounted on them. The rods were rigidly connected with the specimen which means that the angular deformation of the specimen will be directly transferred to the mirrors. Linear scales were placed in front of the mirrors at the same height and at a distance ℓ. The pictures of the scales in the mirrors were focused in high precision theodolites, through which the scales could be read with an accuracy of ± 0.2 mm. As shown in figure 5 an angular change of the mirror will be seen as a vertical displacement δ of the hair line on the scale. The angular change of the mirror (and the specimen) φ is given by

$$\varphi = \frac{1}{2} \cdot \frac{\delta}{\ell} \qquad (2:1)$$

The distance ℓ, which was measured in every individual test with a measuring tape, was about 4 m, which gives a theoretical accuracy for the angle φ of $\pm 2.5 \cdot 10^{-5}$ radians or $\pm 1.4 \cdot 10^{-3}$ degrees. The actual accuracy might be of this order of magnitude in the tests performed at ambient conditions. For the tests at high temperatures additional errors are introduced, such as diffraction due to hot air currents, movements due to thermal dilatation in the connection between the steel rod and the concrete, thermally induced vibrations etc. These problems are most marked at varying temperatures. However, under these conditions the measured values are also greater and the observed reproducibility indicates that the relative errors are of the same order of magnitude under all conditions.

2.5 Heating and Transient Temperature Distribution in the Specimens

The heating of the specimens was provided by an electrical furnace with an effect of 15 kW (figure 6). The walls are made of refractory bricks and the heating elements consist of spirals made of a high-

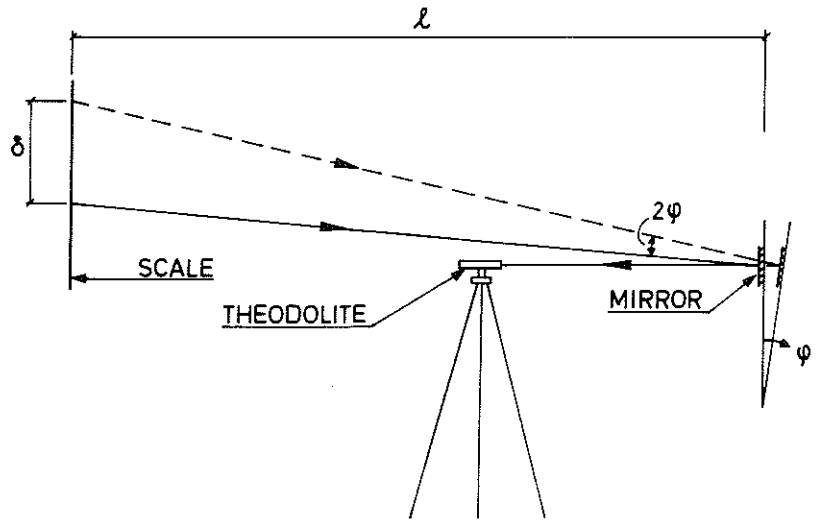

Figure 5. Principle for twist measurements.

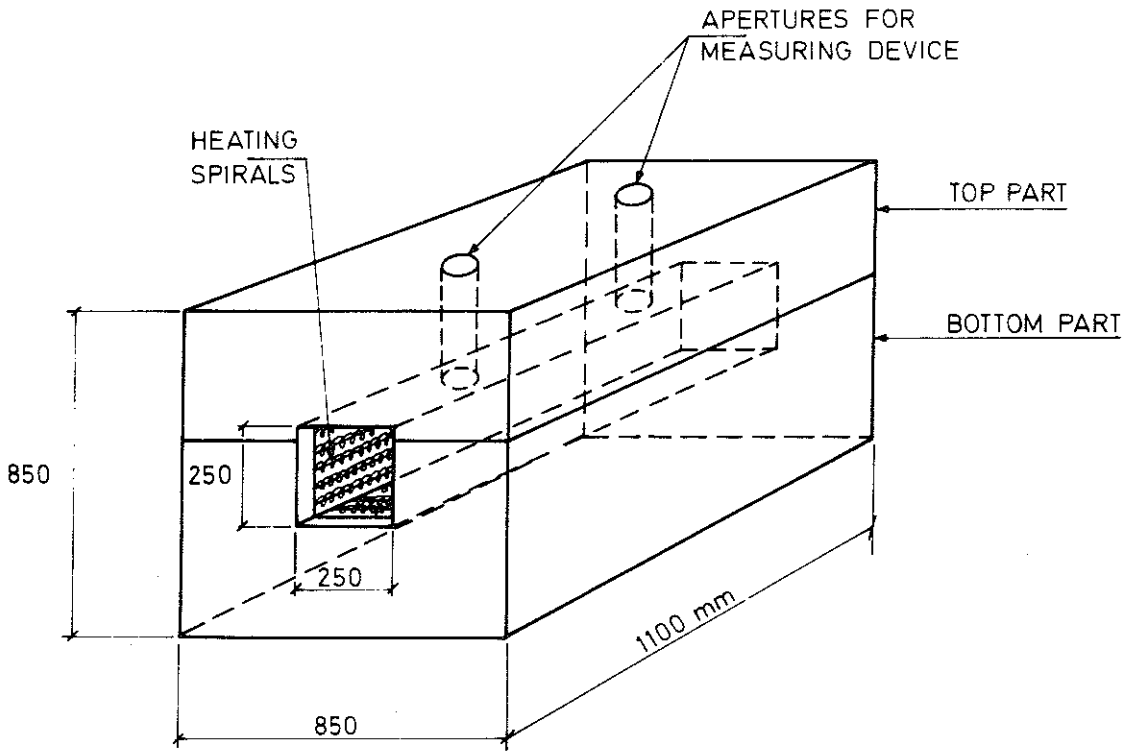

Figure 6. Furnace.

temperature alloy of the type KANTHAL DSD. It is possible to separate the furnace into two parts, top and bottom, to facilitate the mounting of the specimen. The position of the specimen in the furnace under testing is indicated in figure 4a and b. The furnace is open at both ends and the ends of the specimen with the loading and support devices are situated outside it. To avoid leakage of heat, insulation of mineral wool and asbestos was applied at the ends of the furnace and at the holes in the top. In doing this it was ensured that the loading and measurement systems were not disturbed.

The furnace temperature was regulated by an automatic programming device, capable of following an arbitrarily chosen time-temperature curve. The programming unit consists of a curve follower (Leeds & Northrup, type Trendtrak), a temperature recorder (L & N, Speedomax H) and a proportional band control unit (L & N, D.A.T. Series 60). The proportional band action means in effect that the durations of "on" and "off" times in the furnace vary within a specified interval around the set temperature in proportion to the difference between the set temperature and the actual working temperature. In this way oscillations are avoided and within the limits set by the furnace characteristics a desired time-temperature curve is followed with an accuracy of approximately ± 20°C.

The thermocouple connected to the programming unit was placed on the top of the specimen in the mid section in contact with the surface but unprotected. The temperature measured in this way is slightly higher than the "true" surface temperature of the specimen, measured in a cast-in thermocouple as shown in figure 7. The temperature measured in an unprotected thermocouple at about 30 mm from the surface is considerably greater, especially at lower temperatures. Furthermore, the temperature exposure is somewhat smaller at the sides of the specimen (curve 2) than on the top. The tendencies shown in figure 7 were typical for the tests, regardless of rate of heating.

The arrangement with the end of the specimen being outside the furnace gives a heat flow in the longitudinal direction. Within that part of the specimen where the measurements are made the variation of the temperatures in the longitudinal direction is practically negligible. This is shown in figure 8, where for test C4 (rate of

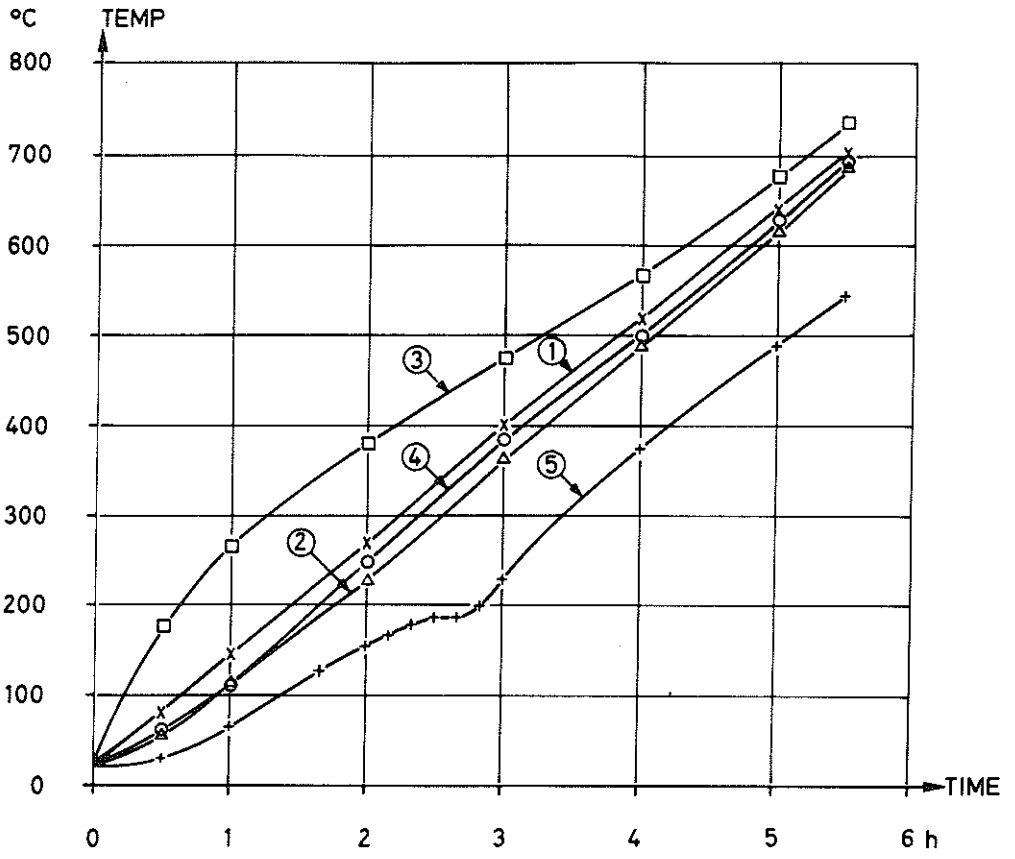

Figure 7. Measured time-temperature relations in a test with a rate of heating of $2\ ^{\circ}C \cdot min^{-1}$.

1. Unprotected thermocouple in contact with the top surface of the specimen.
2. Ditto on the side surface of the specimen.
3. Unprotected thermocouple ≈ 30 mm above the top of the specimen.
4. Cast-in thermocouple less than 1 mm from the surface on the top of the specimen.
5. Cast-in thermocouple 53 mm from the top surface of the specimen.

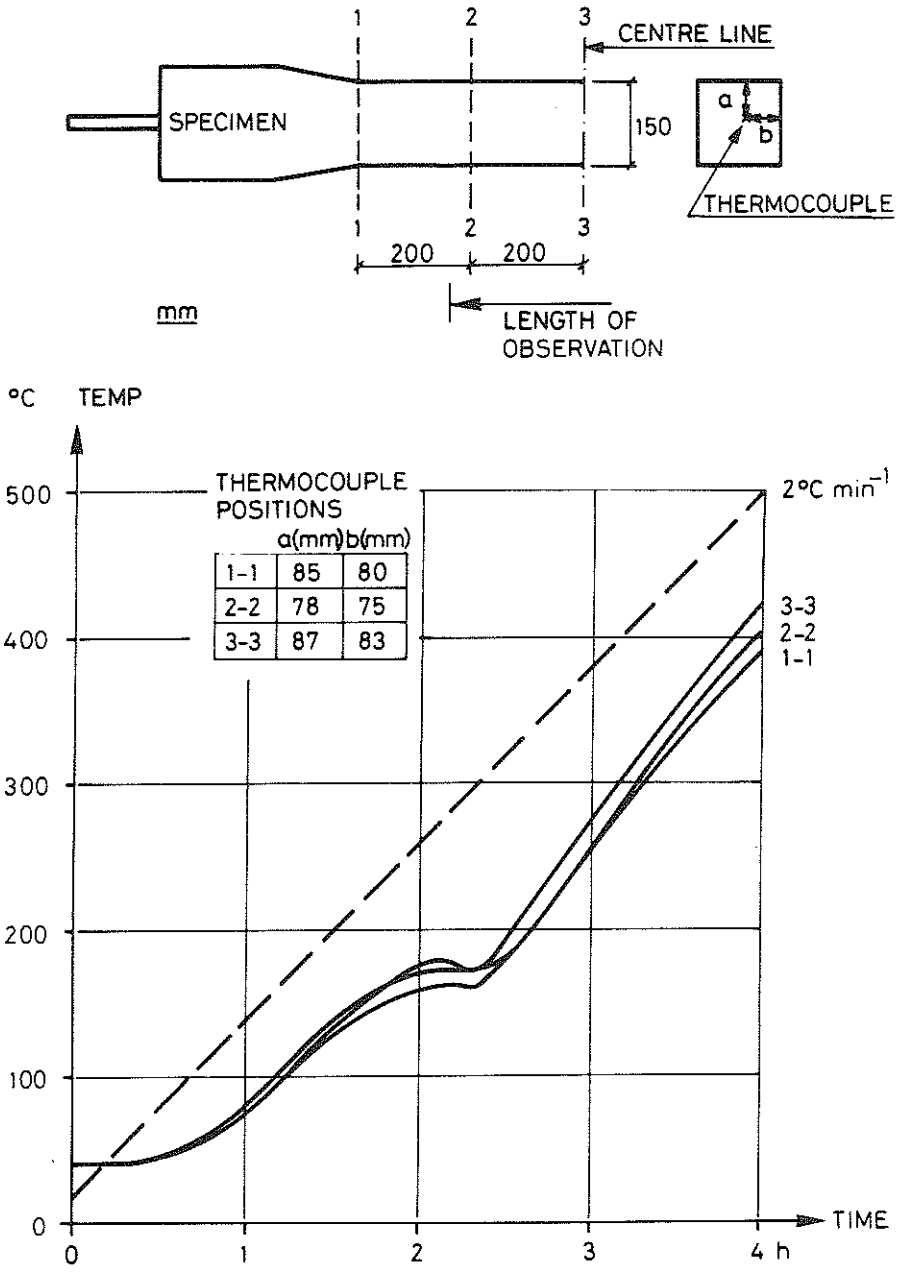

Figure 8. Measured time-temperature relation in test C4, with a rate of heating of $2^{\circ}C \cdot min^{-1}$.

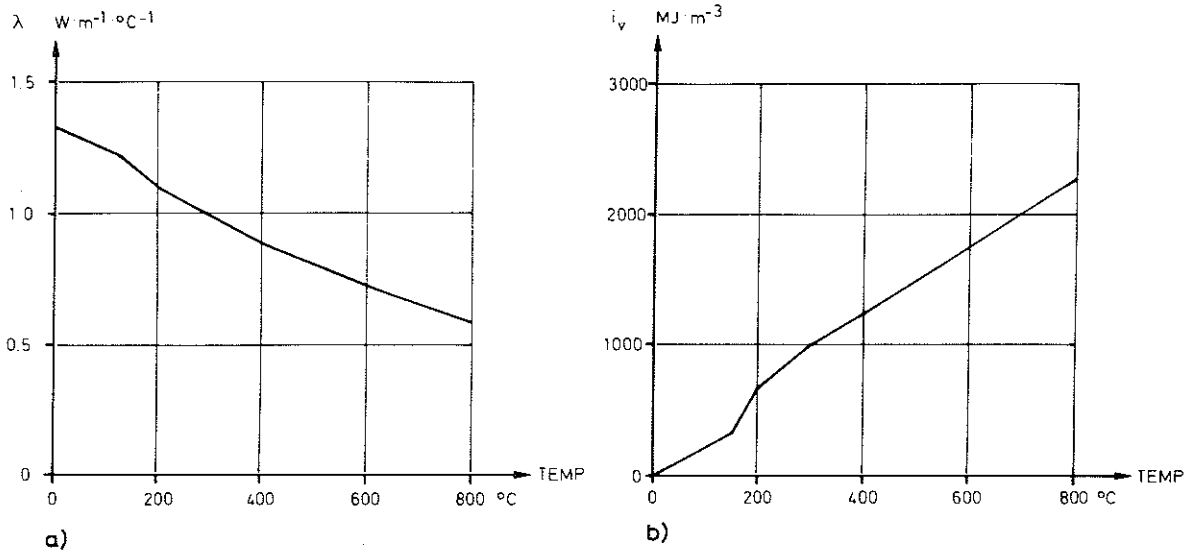

Figure 9. Variation with the temperature of
a) thermal conductivity, λ
b) enthalpy, i_v
used in the temperature calculations.

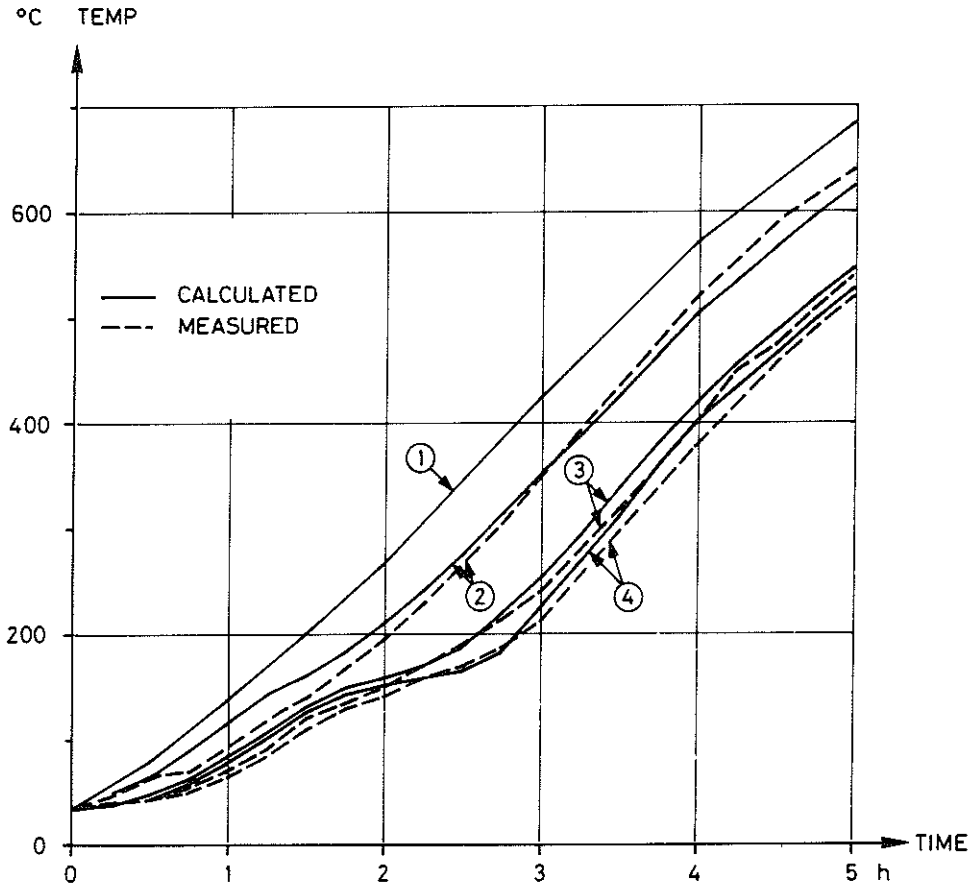

Figure 10. Measured and calculated temperatures in a circular specimen at a rate of heating equal to 2 °C·min⁻¹.
Curve 1: Surface temperature (used as input)
Curve 2: Temperature in r = 60 mm
Curve 3: Temperature in r = 30 mm
Curve 4: Temperature in r = 15 mm
r = distance from centre.

heating $2^{\circ}C \cdot min^{-1}$) the temperatures at different positions along the central axis are given. The difference within the length under observation amounts to $25^{\circ}C$ at most. This difference was found to be even smaller at higher rates of heating.

In every test the temperatures in the specimen were measured in at least 2 points, viz. in the centre of sections 2 and 3 in figure 8. In some of the tests more detailed measurements with several thermocouples at different depths were made. In order to get more detailed information about the temperature distribution a computer program was used to calculate the temperature fields in the specimens with circular cross sections. The computations were made according to the principles given in /11/, and the variation with the temperature of the thermal conductivity λ and the enthalpy i_v used in the calculations are shown in figures 9a and b. The curves are mainly based on measurements made by Ödeen & Nordström /13/, but the enthalpy curve has been modified in the range 100 - $200^{\circ}C$ to take into account the latent heat in the evaporation of the free moisture. This modification was made so as to give the best agreement between measured and calculated temperatures.

An example is shown in figure 10, where measured and calculated temperatures in the interior of the specimen are compared. It was clearly verified from this and other tests that the computer program was capable of simulating the transient heat flow into the circular specimens.

In this way the temperature distributions in the specimens could be theoretically determined in detail in the different tests, and the measurements in single points could be used as a check on the reliability of the calculated temperature fields. In figure 11 is shown the transient temperature fields for circular specimens heated at the rates 2, 4 and $8^{\circ}C \cdot min^{-1}$ respectively.

The temperature distributions have been discussed in relative detail, due to the fact that they are used as a basis for the theoretical analysis in chapter 4.

To investigate the influence of the evaporable water on the thermal performance three circular specimens without any statical load were

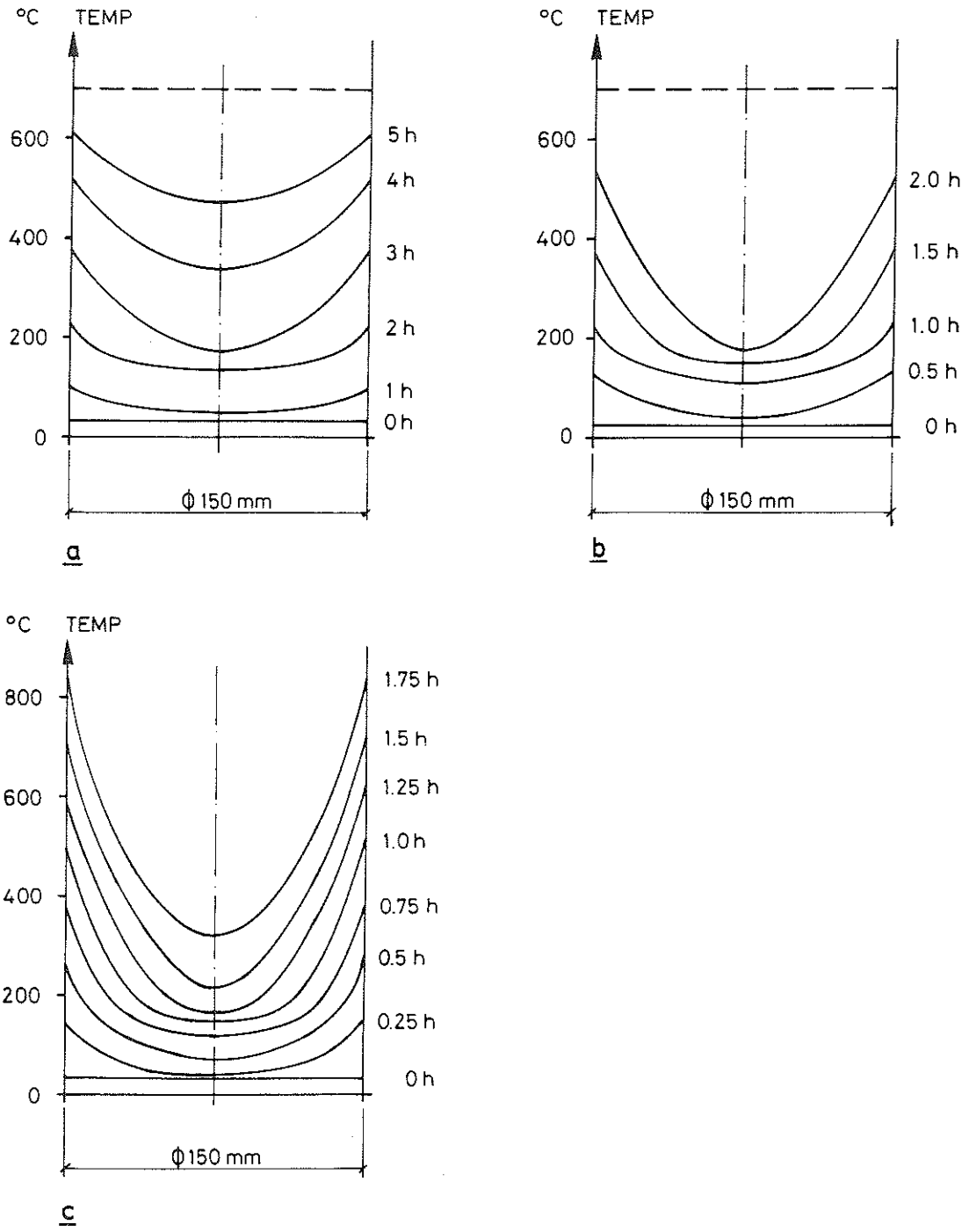

Figure 11. Calculated temperature distribution in the circular specimens at different times from the start of heating.
a) Test C1, 2 °C·min^{-1}
b) Test C10, 4 °C·min^{-1}
c) Test C12, 8 °C·min^{-1}

heated at the rates 2, 4 and 8°C/h respectively. The temperature was measured in a number of points, and an attempt was also made to measure the steam pressure inside the specimens, using a technique developed in USSR /14/. The steam pressure gauge consists of a water-filled copper tube (inside diameter 1.5 mm) connected to a spring manometer. The pressure measured in this way is probably not quantitatively relevant but may be used for qualitative comparisons.

The results from these tests are shown in figure 12. As indicated in the figure the specimens heated at 4 and 8°C · min^{-1} exploded violently after a certain time. The explosions happened when the temperature increase in the central part of the specimen became stagnant, i. e. when the evaporation of moisture took place. The measured pressures attain their maximum values at the same time, these values being greater for higher rates of heating. Evidently, the explosions are caused by excessive steam pressure.

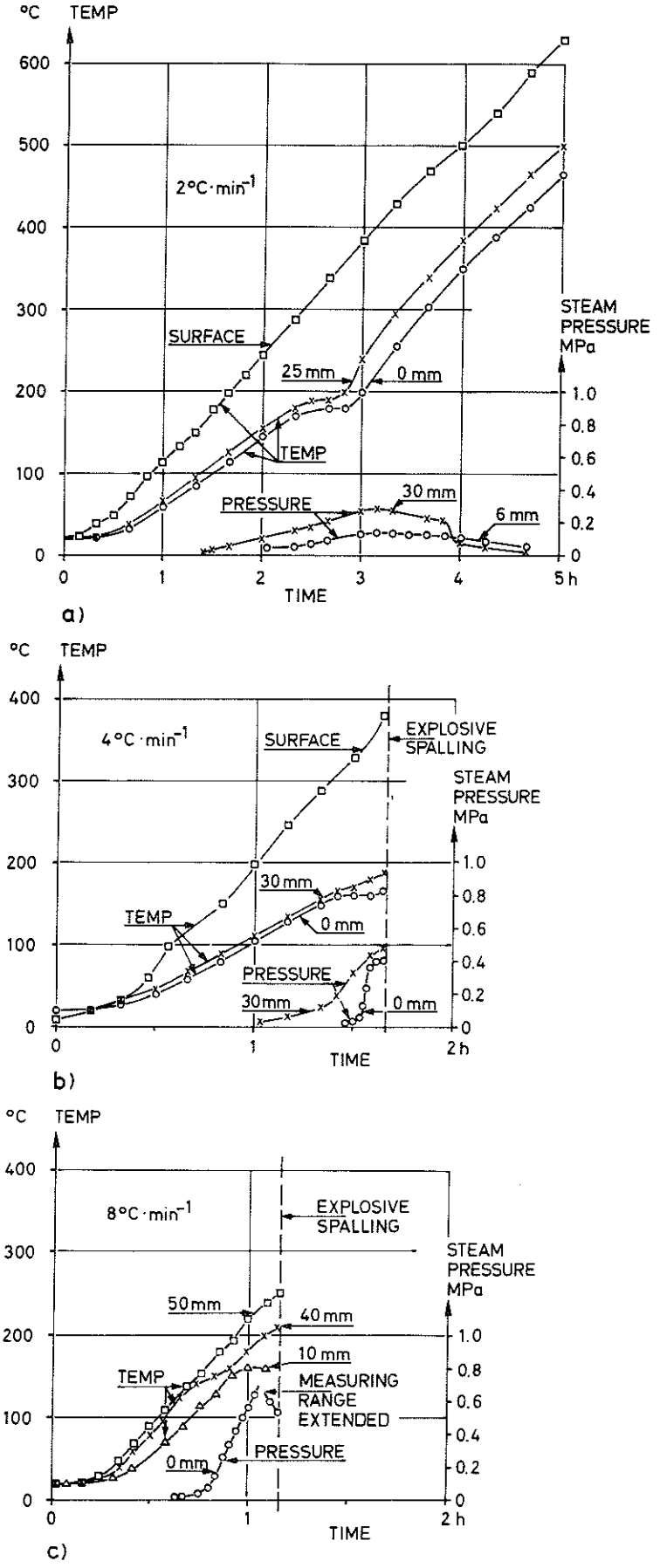

Figure 12. Temperature and steam pressure measured in different points of the specimen as a function of time. On the curves are indicated the respective distances from the centre.

a) $2\,^{\circ}C \cdot min^{-1}$
b) $4\,^{\circ}C \cdot min^{-1}$
c) $8\,^{\circ}C \cdot min^{-1}$

3. Test Results

3.1 Ultimate Torque

The ultimate torques obtained under loading to failure for the different tests are given in table 1, section 2.1. In figure 13 the ultimate torques at different test temperatures are given in % of the ultimate torque at 20°C. Each point represents one specimen. The reference value at 20°C has been obtained from the tests A1 - A6, and all percentages are adjusted in proportion to the split-cylinder strengths of the respective batches. The scatter is considerable, especially for the tests from series B and D. For the sake of comparison, curves for split-cylinder tensile strength (curve 1) and flexural strength (curve 2) at various temperatures have been included. Curve 1 was taken from /15/ and refers to the same concrete as was used in the torsion tests. Curve 2 for the flexural strength /16/ refers to concrete with gravel aggregates and similar mix proportions (cement: aggregate = 1:6.8, W/C = 0.62). As far as the tests from series A are concerned the torsional strengths in almost all cases fall between the two curves for split-cylinder and flexural strengths. In the tests from series B and D, where the specimens were loaded to failure after being subjected to creep tests, a markedly high strength was observed in the range 200 - 300°C. This is difficult to explain but one reason might be that these specimens were subjected to a longer heating, which could give an increased hydration in the temperature range in question. It is not very likely that the presence of load during the creep test could have increased the strength. Nor can the difference be attributed to the different loading procedures, stepwise loading in the series A and continuous increase of the load in the series B and D. If that were the case the difference ought to be similar at all temperatures.

Curve 3 in figure 13 represents the relation between strength and temperature used in the theoretical analysis, see chapter 4.

A direct comparison between the torsional strength of circular and square specimens can give an indication of the type of failure. Plotting the ratio between the ultimate torques for square and circular sections, $M_{tu}^{sq}/M_{tu}^{circ}$, against temperature we obtain the results shown

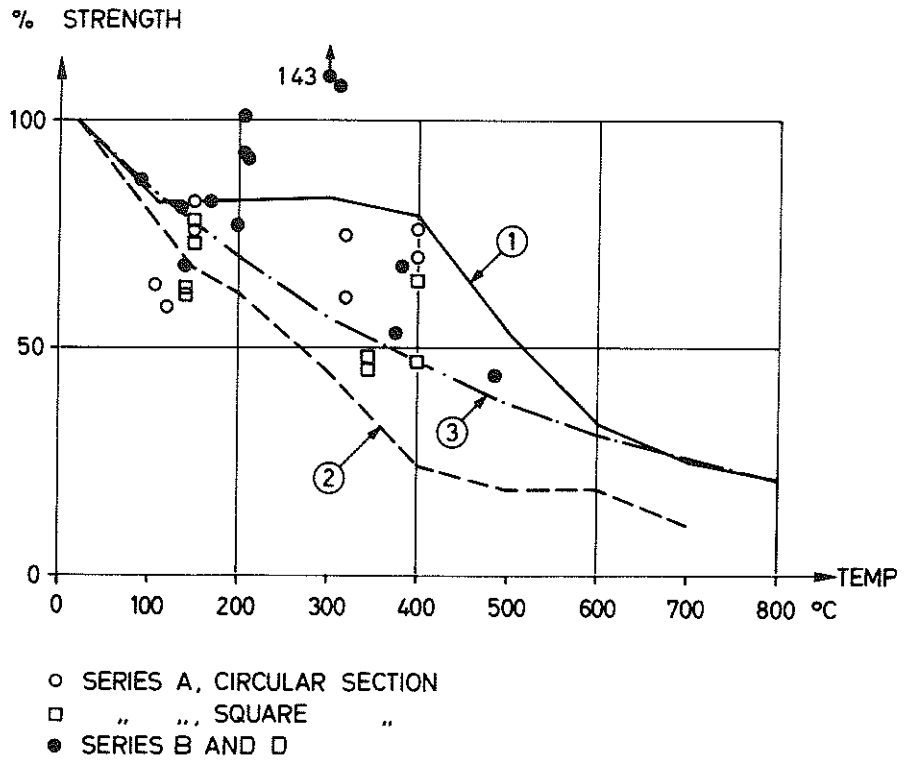

Figure 13. Effect of temperature on the ultimate torsional strength. Each point represents one specimen tested. The results are compared with relative split-cylinder tensile strength (curve 1) and flexural strength (curve 2). Curve 3 represents the relation used in the theoretical analysis in chapter 4.

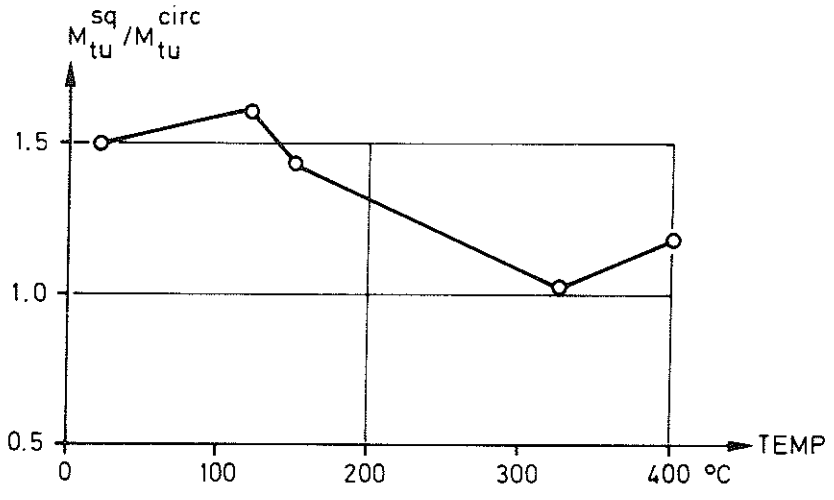

Figure 14. The ratio between the ultimate torques for square and circular specimens as a function of temperature.

in figure 14. If elastic theory according to de Saint-Venant is valid this ratio will have the value 1.06 while, if plastic theory is applicable the value will be 1.26. As seen from figure 14, the ratios obtained in the tests at lower temperatures are considerably higher than both of these values. This is in agreement with tests at ambient conditions accounted for in literature, where ratios between rectangular or square beams and circular beams corresponding to $M_{tu}^{sq}/M_{tu}^{circ} = 1.54 - 1.66$ were obtained /17/. These high values are in accordance with a theory by Hsu /18/ for the torsion of plain concrete. According to this theory the failure of rectangular and square specimens in torsion occurs by bending about an axis parallell to the wider face and inclined at an angle of 45° to the longitudinal axis of the specimen. The component of the torsional moment vector parallell to this axis constitutes the effective bending moment. With this mechanism of failure and under the assumption of elastic conditions the ratio in question would be 1.70. Hsu's theory gives markedly higher ultimate torques for rectangular specimens than the classical theories, while for circular specimens the same results are obtained.

At higher temperatures (300 - 400°C) the ratio $M_{tu}^{sq}/M_{tu}^{circ}$ is smaller ($\approx 1.0 - 1.2$) and hence in agreement with classical torsion theory. The meaning of this is difficult to assess but the mode of failure is probably different for the square section at these temperatures.

3.2 Torque v.s. Twist

From the test series A torque v.s. twist curves were obtained at different temperatures. These are shown in figure 15 for both square and circular specimens. The curves are not quite linear up to failure, indicating that non-elastic deformations develop to some extent, this being more pronounced at high temperatures. It is rather difficult to determine the shear modulus in a unique way from these torque-twist curves, and it was decided to study the secant modulus at 30 % of the ultimate load at 20°C, i.e. approximately 650 Nm for the circular and 1000 Nm for the square specimens. The same absolute stress level was used at all temperatures.

The shear modulus defined in this way was calculated at different temperatures for the tests of series A, but also in the tests of

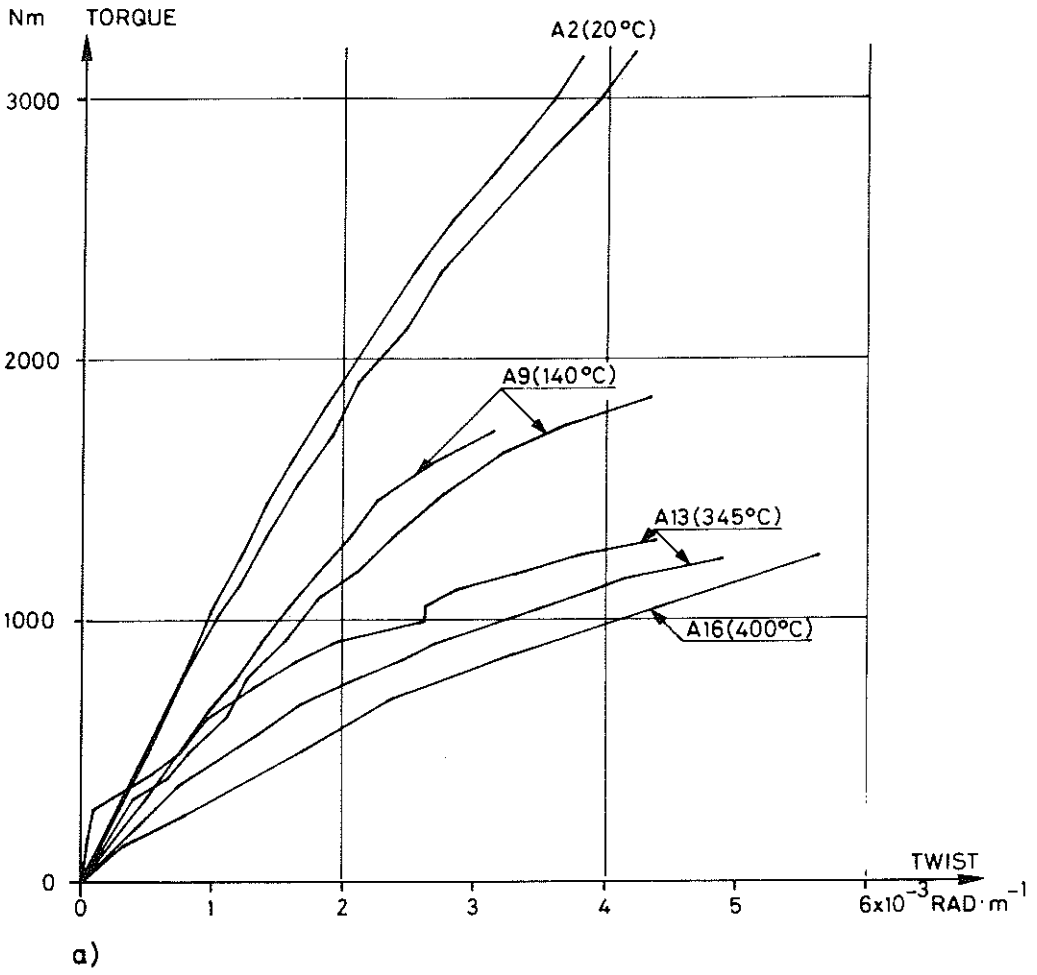

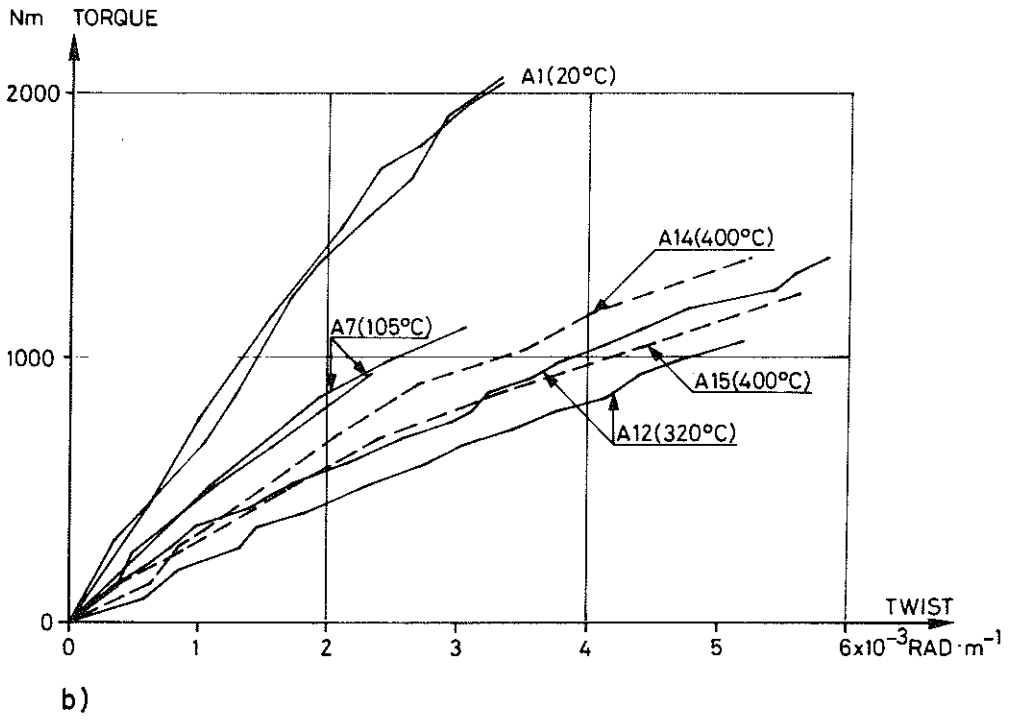

Figure 15. Torque-twist curves for different temperatures.
a) Square sections.
b) Circular sections.

series B on the basis of the deformations measured under the initial loading of the specimens.

The shear modulus G_o at 20°C was determined from a total of 30 tests mainly from the series C and D, where the specimens were loaded before heating. The average value of G_o was $1.22 \cdot 10^4$ MPa for circular (24 tests) and $1.48 \cdot 10^4$ MPa (6 tests) for square specimens. It is often assumed that the elastic modulus of concrete is proportional to the squareroot of the compressive strength and in an attempt to correlate the cube strength (σ_{cube}) of different batches with the observed values of G_o these were plotted against $\sqrt{\sigma_{cube}}$ in figure 16. Although the dispersion is large the best straight line through origin was determined for the square and the circular specimens as shown in the figure. The coefficients of variation were 15 and 26 % respectively.

In figure 17 the ratio between the shear modulus G_θ at different temperatures and the original modulus G_o is shown as a function of temperature. The values have been corrected for the difference between the batches on the basis of the straight lines in figure 16. Curve 1, which has the equation

$$\frac{G_\theta}{G_o} = \exp\left[-2.64 \cdot 10^{-3} \cdot (\theta - 20)\right] \qquad (3.1)$$

has been obtained from regression analysis of the data. The exponential expression was found to fit well with the data. For the sake of comparison a curve for the dynamic shear modulus obtained by Cruz /19/ on siliceous aggregate concrete with similar mix proportions has been included in the figure. As could be expected, curve 1 expressing the static modulus shows somewhat lower percentages than Cruz's curve.

3.3 Constant Temperature Creep

The time-dependent deformation under load at constant temperature, termed constant temperature creep, is measured in the test series B. The results are shown in figure 18, where the creep under a load equal to 30 % of the original ultimate load is plotted against time. The time dependence is similar to that of creep under ambient condi-

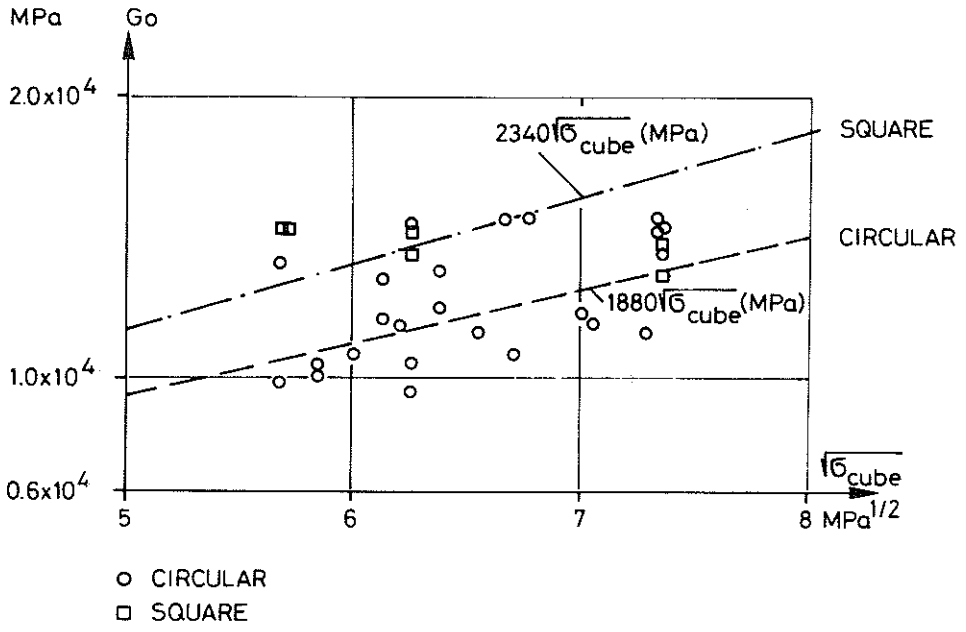

Figure 16. Correlation between the shear modulus G_o measured at ambient conditions and the squareroot of the cube strength.

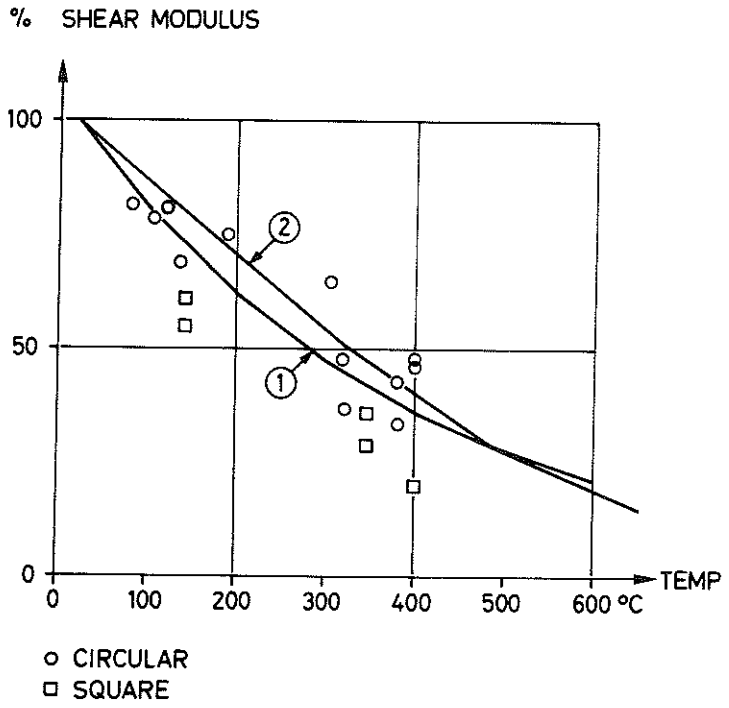

Figure 17. The shear modulus G_θ at different temperatures related to the shear modulus G_o at ambient conditions. Curve 1 shows the exponential curve (eq. 3.1) obtained by regression analysis of the data. Curve 2 shows the dynamic modulus as obtained by Cruz for concrete with siliceous aggregate. (Cylinder strength 42.5 MPa, Cement: aggregate = = 1:4.48, w/c = 0.42 and $G_o = 1.94 \cdot 10^4$ MPa).

tions with the creep rate decreasing with time.

The influence of temperature is illustrated in figure 19a where the ratio φ_{3h} between the creep after 3 hours, $\phi_{c,3h}$ and the instantaneous elastic deformation at 20°C, ϕ_o is plotted against temperature. For each individual case ϕ_o is determined on companion specimens from series D made from the same batch. The creep increases monotonically with the temperature above 135°C and attains at 400°C a value approximately twice as great as the elastic deformation at 20°C. The value obtained at 80°C is comparatively high, which may depend on the presence of moisture at this temperature.

The temperature dependence is qualitatively very similar to that obtained by Marechal /20/ for creep in compression on unsealed saturated specimens, see also /6/ p. 19.

The temperature dependence of creep in different materials including cement paste and concrete is often formulated in terms of the Arrhenius activation energy equation, giving the following relation

$$\dot{\varepsilon}_c \sim \exp\left(-\Delta H/RT\right) \qquad (3.2)$$

where $\dot{\varepsilon}_c$ = creep strain rate
ΔH = activation energy for creep, J/mole
R = gas constant, J/mole · K
T = absolute temperature, K

The value of $\Delta H/R$ can be obtained from the so called Arrhenius plot, i.e. $\ln\dot{\varepsilon}_c$ vs $\frac{1}{T}$. In this connection the ratio $\varphi_{3h} = \phi_{c,3h}/\phi_o$ is assumed to be a measure on the creep rates at different temperatures and in figure 19b in φ_{3h} is plotted against 1/T. Except from the value at 80°C the points form a straight line with small scatter. If the point at 80°C is omitted we obtain by regression $\Delta H/R$ = 1620 K. The curve corresponding to the regression line is shown in figure 19a.

Marechal /20/ found values of $\Delta H/R$ in the range 1600 to 1960 K for creep in compression of concretes with different aggregates. These values are of the same order of magnitude as that obtained from the relation between temperature and viscosity of free water ($\Delta H/R$ = = 1756$^{\phi}$K), cf /21/.

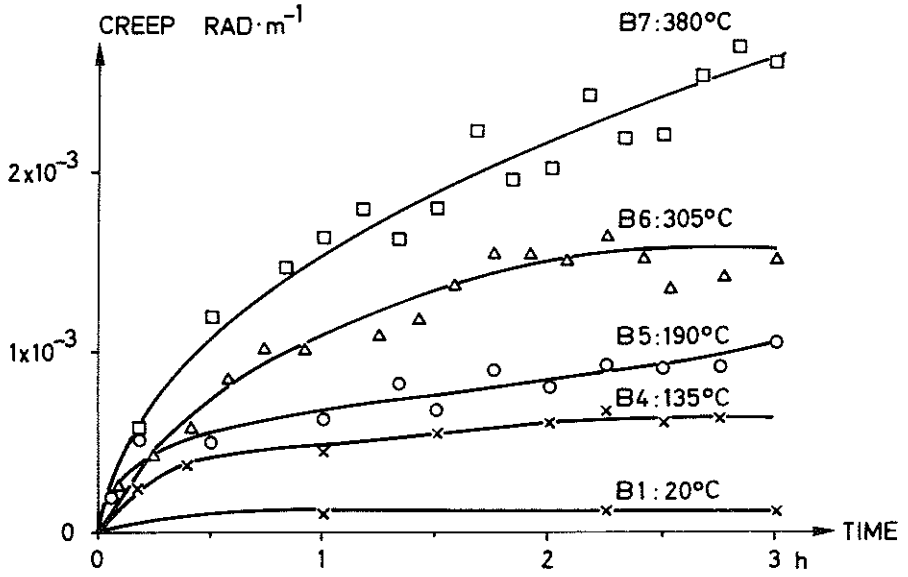

Figure 18. Creep at different constant temperatures as a function of time. The load was equal to 30 % of the ultimate load at 20°C.

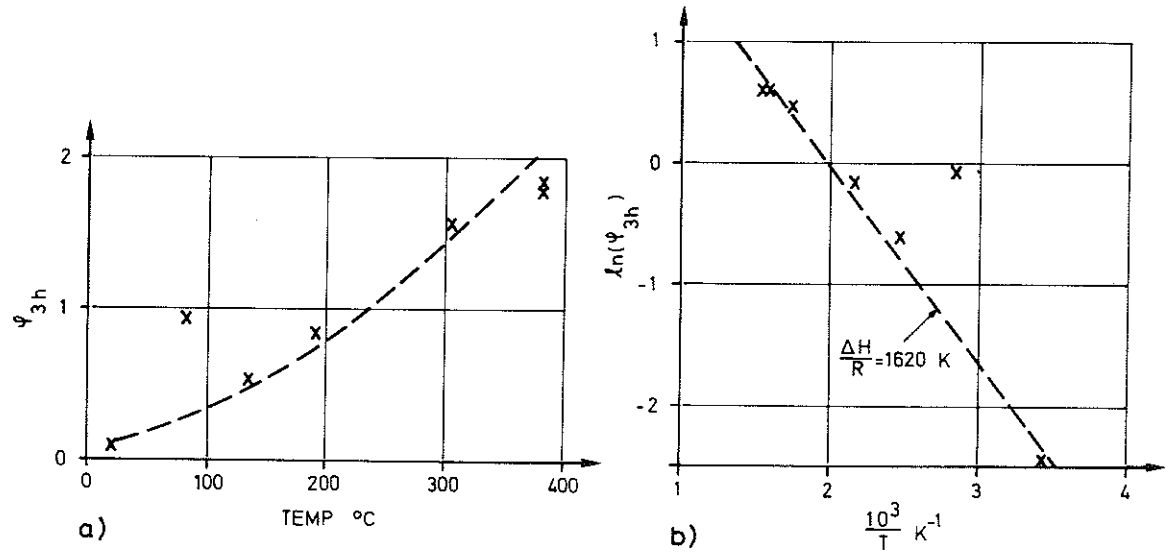

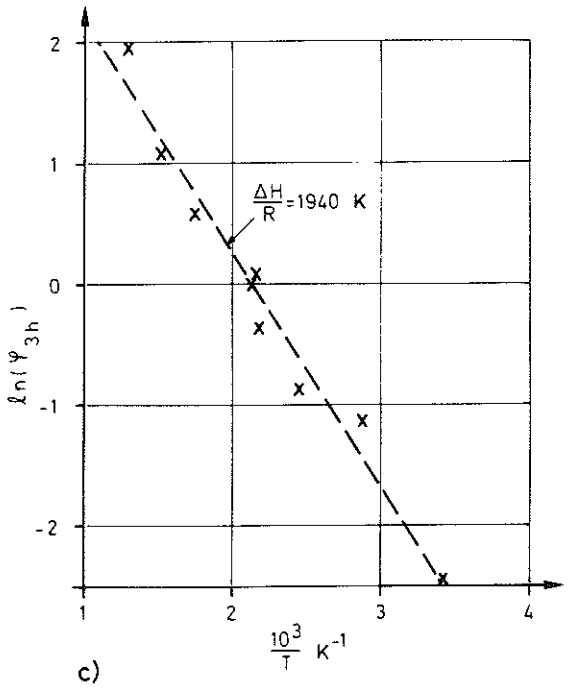

Figure 19. a) The ratio φ_{3h} between the 3h creep in series B and the instantaneous elastic deformation at 20°C as a function of temperature.
b) Relation between ln φ_{3h} and 1/T for the tests in series B.
c) Ditto for series D.

Deformations at constant temperature can also be evaluated from the tests in series D. The difference compared with series B is that the load is applied before heating. $\phi_{c,3h}$ is obtained as the change in deformation during the last three hours of the tests in series D. In figure 19c ln φ_{3h} is plotted against 1/T, the regression line having a slope corresponding to $\Delta H/R = 1940$ K.

Accordingly, the deformations in this case are on the average somewhat greater than those in test series B. The difference is most marked for temperatures above 350°C.

3.4 Deformations under Transient Conditions

The tests in series A and B were made under constant temperatures, i.e. the specimens were heated prior to the application of load. In the test series C and D the load was applied from the beginning and the specimens were heated until failure occured (series C) or to a maximum temperature level (series D).

It is immediately clear that the deformations under transient conditions are much greater than under constant temperatures. In figure 20 is shown a comparison between tests B7 and D8, which are subjected to identical temperature exposure (figure a). In the first case, B7, the load was applied after the maximum temperature was reached while in the second case D8 the load was applied before heating commenced. In test D8 large deformations occur, mainly under that period when the temperature increases. Obviously we have a "temperature change effect" similar to that found in /7/ and /8/.

This effect is very marked at higher temperatures and the deformations under changing temperature form the most important part of the total deformation.

Similar differences between deformations at transient and constant temperatures were found at all temperature levels tested, except at 70°C where the deformations were of the same order of magnitude in both cases (tests B3 and D1), cf 3.3.

Though part of the deformations of specimen D8 in figure 20 can be attributed to drying creep, the main part must be connected with the

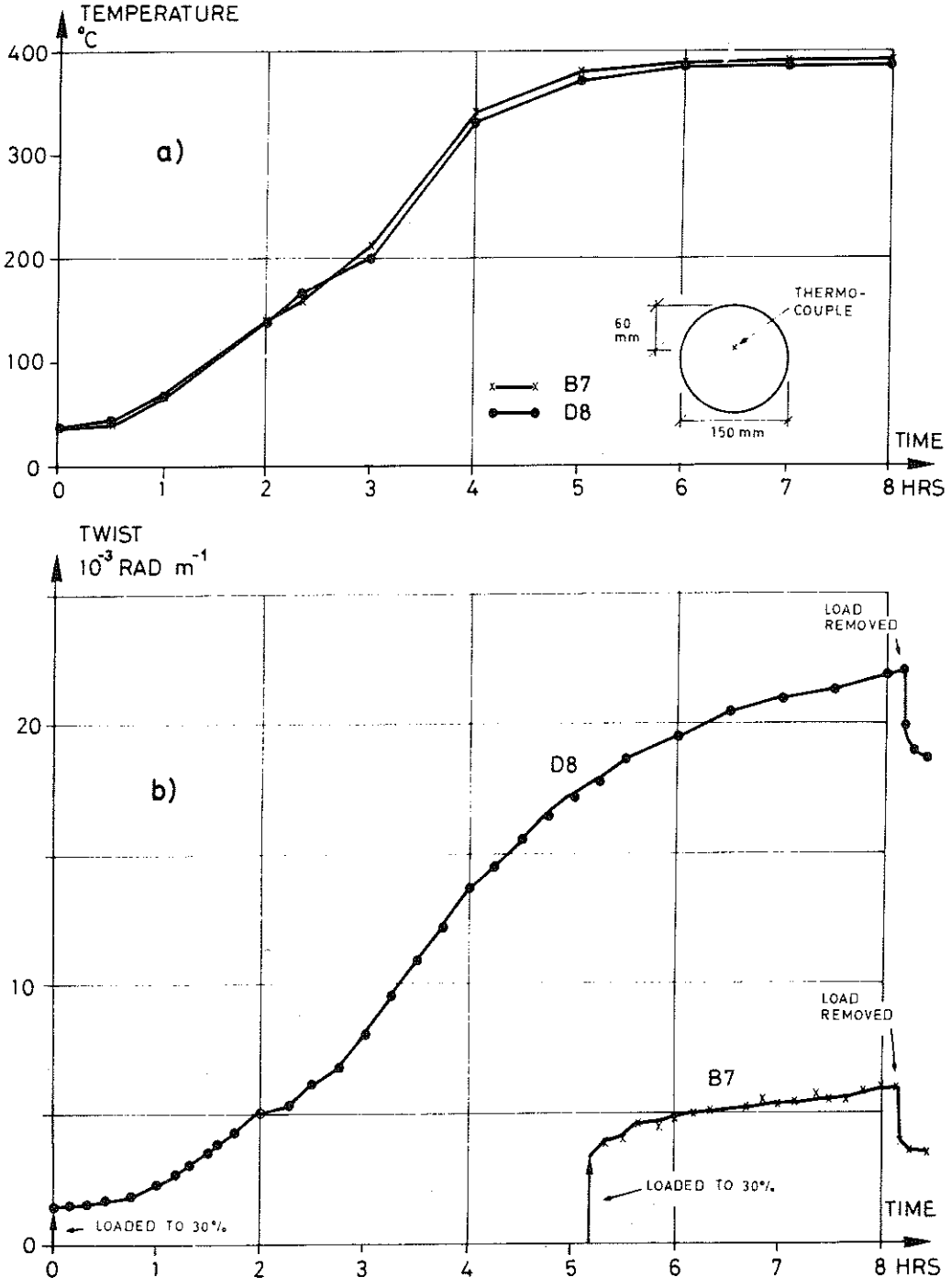

Figure 20. a) Measured temperatures 60 mm from the top surface in the tests D8 and B7 as a function of time.

b) Measured angles of twist as a function of time when the load is applied from the beginning (D8) and after the maximum temperature is attained (B7). The load is equal to 30 % of the ultimate load at ambient temperature.

temperature increase in one way or another. A definite physical explanation of the temperature change effect has not been produced as yet. The phenomenon can hardly be explained as a result of the thermal incompatibility between cement paste and aggregate, since the same effect has been found for neat cement paste /7/.

A probable explanation is instead that the temperature increase suddenly activates physical and chemical reactions in the cement paste. At lower temperatures the temperature change can induce a rearrangement of water molecules in the cement gel, even if the external moisture conditions are constant, and this can strongly affect the deformation behaviour. Especially at higher temperatures but also at lower temperatures the temperature increase gives rise to a suddenly increased rate of chemical decomposition of the cement paste. When this disintegration takes place under sustained stress, the material may undergo deformations, which do not occur if the stress is applied after the reactions have slowed down. If this explanation holds the transient strain is not time-invariant, but is in some way or another connected to the rates of chemical reactions and their temperature dependence. For instance if the rate of heating is sufficiently high the reactions in question will not have time to develop and the temperature in itself will not be a relevant parameter to describe the state of the material. It seems however that the kinetics of the reactions of heated cement paste is such that the activity decreases very soon after a temperature increase. Hence for practically possible rates of heating the state of the material can approximately be related to temperature level. This is reflected in the fact that the strength of concrete at a certain temperature is nearly independent of the rate of heating and the time of exposure. For instance if concrete specimens under sustained stress are heated to failure the temperature at failure is virtually independent of the rate of heating /22/.

In view of the above discussion it seems reasonable to treat the transient strain as a quasi-instantaneous response to a temperature increase, though part of the strain may in fact be somewhat delayed.

Other results from test series C and D are shown in figures 30 - 31

and appendix A together with theoretically calculated curves, see chapter 4. As regards test series C, it can be seen that in some cases very large deformations occur before failure (appendix A, figure A1). In the tests C1 and C2 the total deformations at failure were greater than $45 \cdot 10^{-3}$ rad $\cdot$ m^{-1}, which is about 14 times larger than the deformation at failure for specimens loaded to failure at 20°C.

These extraordinary deformations were found in the tests with low stress level and slow rate of heating ($2^{\circ}C \cdot min^{-1}$). At higher stress and more rapid heating the failure occured earlier, the deformations were not so large and the critical temperatures were lower. In these cases the deformation at failure was in the range $5 - 10 \cdot 10^{-3}$ rad m^{-1}.

At the rates of heating 4 and $8^{\circ}C \cdot min^{-1}$ the failure always occured before the temperature in the centre of the specimen reached 200°C. This is a consequence of the fact that at these rates of heating explosive spalling occurred even for unloaded specimens, see 2.5. Violent explosions due to high steam pressure did take place also in the tests C7 and C8. Also in cases where direct explosive spalling did not occur, the steam pressure may have affected the failure of the specimen. In almost all cases the failure occurred when the temperature increase in the core of the specimen became stagnant, i.e. when the evaporation of the moisture took place.

To make it possible to discuss the tests in series C and D in terms of temperature levels despite the fact that the temperature varies along the thickness of the specimen, the temperature at a fixed distance from the centre is assumed to be representative for the specimen as a whole. The choice of the distance is made so as to account for the distribution of stresses in the cross section. In figure 21 the stress volume for a sector of the circular section is illustrated under two different assumptions, viz. linear elastic (figure a) and perfectly plastic stress distribution (figure b). The centroids of the stress volumes are located at 0.75 R_o and 0.67 R_o respectively. Assuming that the actual stress distribution is something in between these two alternatives, 0.7 R_o is chosen as the characteristic point for the circular specimens.

Though this way of defining a characteristic temperature implies a considerable simplification, it may be useful for a preliminary ana-

lysis. Thus, in figure 22 the deformations at different rates of heating and for two load levels have been plotted against the temperature defined in this way. For the lower stress level the deformations vs. temperature are approximately independent of the rate of heating, whereas for the higher stress level the curves diverge somewhat. In spite of this divergence it can be concluded that the main part of the deformation occuring under heating can be regarded as independent of time.

The results shown in figure 22 also indicate that the deformations are linearly related to the load level, at least for temperatures below 200°C. The same conclusion can be drawn from figure 30, which shows the deformation vs. time for 4 different load levels, all other things being equal. In figure A5 (se Appendix A), however, where the tests D3 - D6 are shown, the effect of the load is irregular. This may be explained by the fact that in these tests the temperature in the concrete is stabilized on a level where the evaporation of moisture takes place, which gives unstable moisture conditions and bad reproducibility of the temperature conditions.

Another reason in this particular case seems to be the variation of concrete properties between the specimens; as seen from the figure the initial deformation (t = 0) is approximately equal for the tests D4, D5 and D6 in spite of the different load levels.

3.5 Deformations upon Unloading

In series B and D the load was removed at the end of the test and the deformation was studied during 15 minutes. The deformations measured in this way are shown in figure 20 for the tests B7 and D8. The total decrease in deformation due to unloading is of the same order of magnitude in both cases, a conclusion which applies to all temperature levels. This is shown in figure 23, where the total decrease in deformation due to unloading is plotted against temperature for the tests from series B and D (curve 1 and 2 respectively). In the figure has also been plotted the instantaneous deformations obtained when the load was applied at different temperatures (series B). All three curves are very close to each other, indicating that the deformations under changing temperature as well as the main part of the constant temperature creep are irrecoverable. The

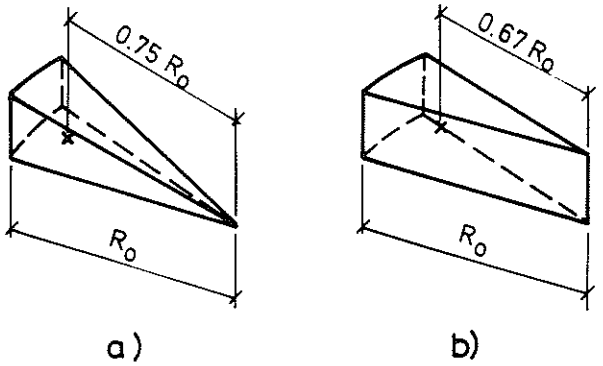

Figure 21. Stress volumes for circular cross section under torsion.
a) Elastic stress distribution.
b) Perfectly plastic stress distribution.

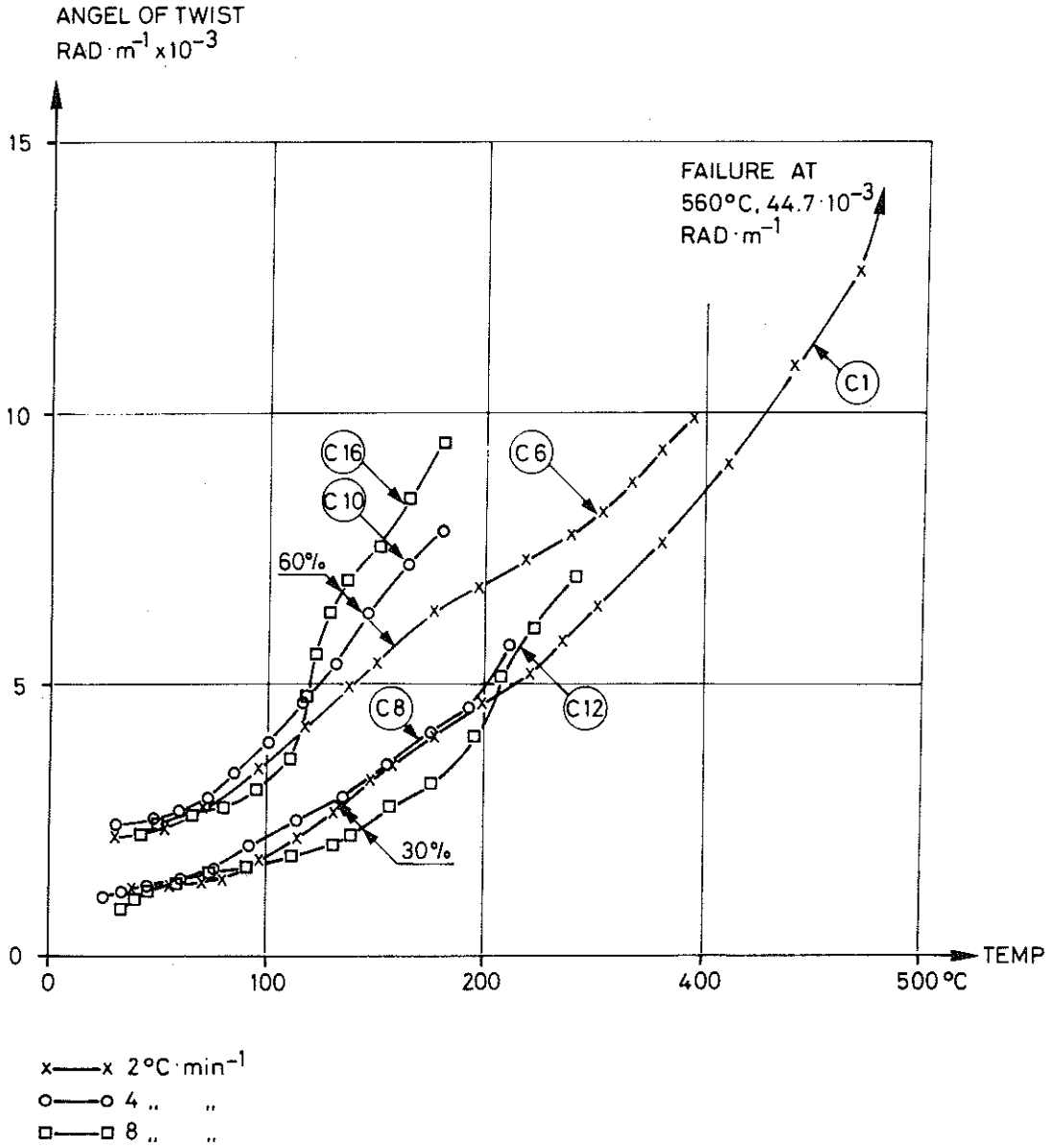

Figure 22. Angular deformations under transient temperature conditions as a function of the temperature at the distance 0.7 R_o from the centre of the specimen.
R_o = radius of circular cross section.

recovery during the period after 15 minutes has not been studied but in one test, viz. D1, where no significant change in deformation was found beyond 15 minutes. For the present purpose it will be assumed that the instantaneous response to a load is elastic while the rest of the deformation is plastic.

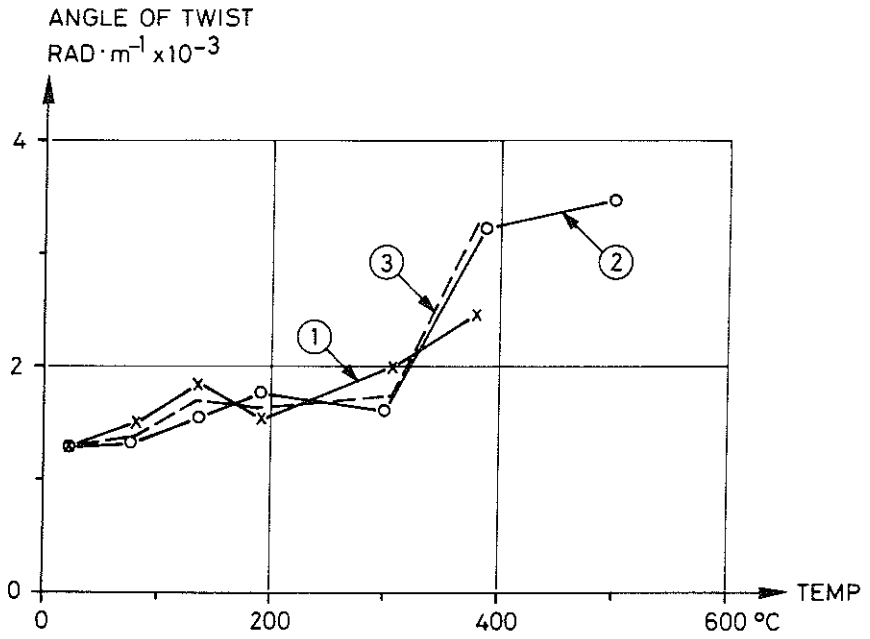

Figure 23. Total decrease in deformation due to unloading including recovery during 15 min. The load level was equal to 30 % of the ultimate load at 20°C.

Curve 1: Test series B, load applied after heating.

Curve 2: Test series D, load applied before heating.

Curve 3: Instantaneous strain upon loading at different temperatures (series B).

4. Theoretical Analysis

In this chapter a mathematical model of the mechanical behaviour of heated concrete is formulated and shear stresses and strains are calculated for the twisted cross sections. The treatment is limited to the circular case, where the axisymmetry gives a simple stress distribution. The equilibrium, compatibility and constitutive equations are written down, the latter on the basis of the test results described in section 3. The method of calculation is described and the angular deformations obtained from the theory are compared with the results from the test series C and D.

It will be assumed throughout that the thermal stresses developed under transient conditions do not affect the shear stress distribution imposed by the torsional moment. This would be exactly true if the material were elastic and must be regarded as a reasonable assumption also under the present circumstances.

4.1 Equilibrium Equation

From the axisymmetry follows that the shear stress τ is a function of the distance r from the centre and constant on any circle concentric with the boundary. The equilibrium equation is written

$$M_t = 2\pi \int_0^{R_o} \tau \cdot r^2 dr \qquad (4.1)$$

where

M_t = torque applied at the section, Nm

τ = shear stress, Pa

r = distance from the centre, m

R_o = radius of the circular cross section, m

If the cross section is divided into n ring-shaped elements, eq. (4.1) can be rewritten

$$M_t = 2\pi \cdot \sum_{i=1}^{n} \tau_i \cdot r_i^2 \cdot \Delta r_i \qquad (4.2)$$

where

τ_i = shear stress in element i, Pa

r_i = radius of element i, m

Δr_i = thickness of element i, m

4.2 Compatibility Equation

The compatibility equation for a circular cross section is given by

$$\gamma = r \cdot \phi \tag{4.3}$$

where

γ = shear strain, Rad

ϕ = angle of twist per unit length, $Rad \cdot m^{-1}$

Dividing the cross section into n discrete elements yields

$$\gamma_i = r_i \cdot \phi \tag{4.4}$$

where

γ_i = shear strain in element i, Rad

4.3 Constitutive Equation

The constitutive equation gives the relation between shear stress τ and shear strain γ and includes in this case the effects of temperature and time. It is first assumed that a stress τ is applied at $t = 0$ and then held constant i.e.

$$\frac{\partial \tau}{\partial t} = 0 \qquad \text{for } t > 0 \tag{4.5}$$

where t = time coordinate

(Later on principles of superposition will be dealt with, thus allowing $\frac{\partial \tau}{\partial t} \neq 0$).

As long as eq. (4.5) is valid it can be assumed that

$$\gamma = J(\theta,t) \cdot \tau \tag{4.6}$$

where

$J(\theta,t)$ = linear compliance depending on θ and t in MPa^{-1}

θ = temperature in ^{o}C

Eq. (4.6) implies that the basic assumption for linear viscoelasticity theory has been accepted. This assumption gives the most simple stress dependence and is partly justified by the results accounted for in section 3.4, figure 22, which shows that the total deformation is roughly proportional to the load level at least up to 60 % of the original ultimate load. It is furthermore shown in figure 15 that the torque-twist curves are almost linear up to failure. The stress dependence for the constant temperature creep has not been studied herein, but Maréchal /20/ found that the creep in compression was nearly linear with stress up to 400°C for stresses up to at least 50 % of the strength at normal temperatures. At ambient conditions numerous test results indicate that the creep is linear with stress for stress-strength ratios up to 60 % or more.

It may be that the assumption of linear stress dependence does not hold for high stress-strength ratios, but as yet no information is available that can justify an assumption other than the linear. The deformations obtained for high stress-strength ratios may thus be underestimated but this is in effect balanced by the fact that the material is assumed to behave in a perfectly plastic way as soon as the ultimate limit has been reached for the actual temperature, see section 4.5.

Now, the test results can be used to determine the function $J(\theta,t)$. Combining eqs. (4.1), (4.3) and (4.6) we obtain

$$M_t = 2\pi \cdot \phi \cdot \int_0^{R_o} \frac{r^3 dr}{J(\theta,t)} \qquad (4.7)$$

In cases where the temperature is constant over the cross section eq. (4.7) can be written

$$J(\theta,t) = \frac{\phi}{M_t} \cdot 2\pi \cdot \int_0^{R_o} r^3 dr = \frac{\phi}{M_t} \cdot I_p \qquad (4.8)$$

where

I_p = the polar moment of inertia = $\frac{1}{2}\pi R_o^4$.

Eq. (4.8) enables us to compute the value of $J(\theta,t)$ corresponding to a measured angle of twist ϕ.

To determine the function $J(\theta,t)$ we have to separate the total defor-

mation into three different components. The first component is the instantaneous strain obtained as an immediate response to a change in stress. This component is assumed to be fully elastic, cf. 3.5, and is therefore termed elastic strain. The second component is "constant temperature creep" which is the delayed time-dependent response to a change in stress, measured under constant stress and temperature. Finally, the third component is the response to a temperature change in the concrete under stress, here termed transient strain.

Thus the total compliance can be written

$$J(\theta,t) = J_e + J_c + J_t \tag{4.9}$$

where J_e, J_c and J_t are the compliances corresponding to elastic strain, constant temperature creep strain and transient strain respectively.

4.3.1 Elastic Strain

The elastic part of the compliance is a function of temperature only and is given by

$$J_e = \frac{1}{G_\theta} \tag{4.10}$$

where G_θ = shear modulus at the temperature θ. The temperature dependence is given by eq. (3.1), which in combination with (4.10), gives

$$J_e = J_o \cdot \exp\left[2.64 \cdot 10^{-3}(\theta-20)\right] \tag{4.11}$$

with

$$J_o = 1/G_o$$

where G_o = shear modulus at $20^{\circ}C$.

4.3.2 Constant Temperature Creep Strain

This component is very difficult to model mathematically, since it is a function of both time and temperature. But it is also the least important one, which means that rather great approximations can be justified.

The temperature dependence is described by the Arrhenius expression $\exp\left(-\frac{\Delta H}{RT}\right)$, as shown in section 3.3. Assuming that the time functions for different temperatures are affin with each other we can express J_c at constant temperature, $\theta = T - 273$:

$$J_c = f(t)\cdot\exp\left(-\frac{\Delta H}{RT}\right) \tag{4.12}$$

where $f(t)$ = a function of time defining the shape of the creep curve for constant temperature.

Taking the creep curve at a specific temperature $\theta_{ref} = T_{ref} - 273$ as a reference curve we can relate the creep at all temperatures to this curve according to the time-shift principle, see for instance /23/. We define a specific material time t_m, as the required time at the reference temperature to get the same amount of creep as the creep obtained at the actual temperature at the actual time t. Thus at constant temperature $\theta = T - 273$, we get

$$J_c = f(t)\cdot\exp\left(-\frac{\Delta H}{RT}\right) = f(t_m)\cdot\exp\left(-\frac{\Delta H}{RT_{ref}}\right) \tag{4.13a}$$

or

$$f(t_m) = f(t)\cdot\exp\left[-\frac{\Delta H}{R}\left(\frac{1}{T} - \frac{1}{T_{ref}}\right)\right] \tag{4.13b}$$

When $f(t)$ is a known function t_m can be evaluated from eq. (4.13b). If we assume that $f(t)$ is a power function,

$$f(t) \sim t^p$$

where p = constant,
we obtain from eq. (4.13b)

$$t_m = t\cdot\exp\left[-\frac{1}{p}\cdot\frac{\Delta H}{R}\left(\frac{1}{T} - \frac{1}{T_{ref}}\right)\right] \tag{4.14}$$

If the temperature is varying with time we can write

$$t_m = \int_0^t \exp\left[-\frac{1}{p}\cdot\frac{\Delta H}{R}\left(\frac{1}{T} - \frac{1}{T_{ref}}\right)\right]\cdot dt_1 \tag{4.15}$$

where t_1 = time coordinate defined in the interval $0 \leq t_1 \leq t$.

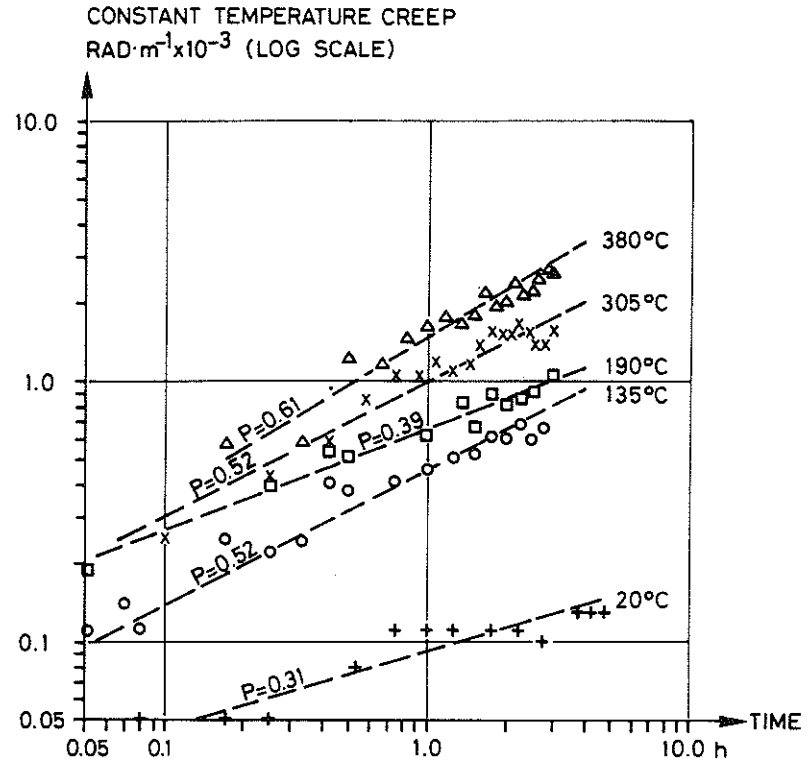

Figure 24. Log - log plot of the constant temperature creep vs. time for different temperatures (series B).

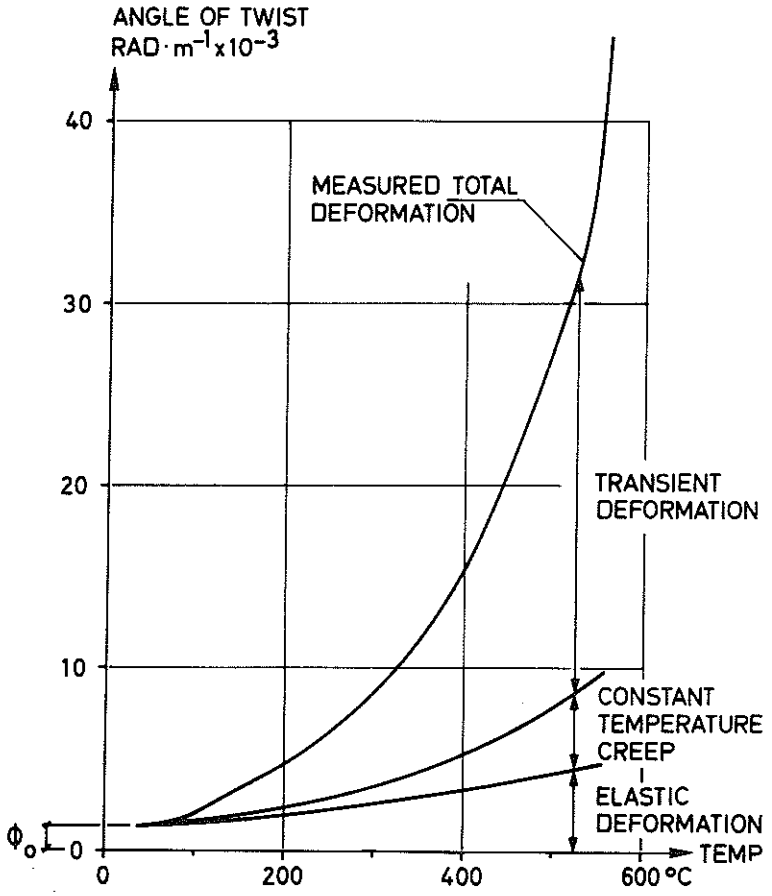

Figure 25. Relation between the different deformation components for test C1. On the abscissa is indicated the temperature at a distance 0.7 R_o from the centre of the specimen.

In this way the temperature history of each point in the material can be transformed into one single parameter t_m, and the compliance J_c is proportional to t_m^p. This can be written in the convenient form

$$J_c = \beta \cdot \left(\frac{t_m}{t_{ref}}\right)^p \cdot J_o \qquad (4.16)$$

where t_{ref} = reference time
β = dimensionless coefficient

Eq. (4.16) together with (4.15) expresses the constant temperature creep component at constant stress, and the different coefficients can be estimated from the test results. Selecting as reference temperature, $\theta_{ref} = 300^{\circ}C$ and reference time, $t_{ref} = 3h$, $\beta \cdot J_o$ is the compliance after 3h at $300^{\circ}C$. From the test results in series B, see figure 19b, we get $\frac{\Delta H}{R} = 1620$ K and $\beta = 1.44$, whereas the results in series D, figure 19c, give $\frac{\Delta H}{R} = 1940$ K and $\beta = 2.14$.

The exponent p can be estimated if the measured constant temperature creep is plotted against time in a log - log diagram. This was done for all the tests in series B (shown in figure 24) as well as series D and the regression lines were determined. As seen in figure 24 the measured values fit well with straight lines. The values of p obtained in this way ranged from 0.31 to 0.69 (the higher value refers to the curve for $80^{\circ}C$, which is omitted in figure 24 for the sake of clarity) for the tests in series B and 0.54 to 0.99 for the tests in series D.

Although the scatter is considerable the assumption p = constant may still be justified. With J_c expressed in the form given by eq. (4.16) the value of p has little influence on the creep after some time (after 3 hours at constant temperature the creep will be independent of the value of p) and the accuracy of the measurements does not justify a more detailed description.

For the calculations the following values were chosen:

$$\frac{\Delta H}{R} = 1780 \text{ K}$$
$$\beta = 1.8$$
$$p = 0.6$$

These values are the averages from series B and D respectively.

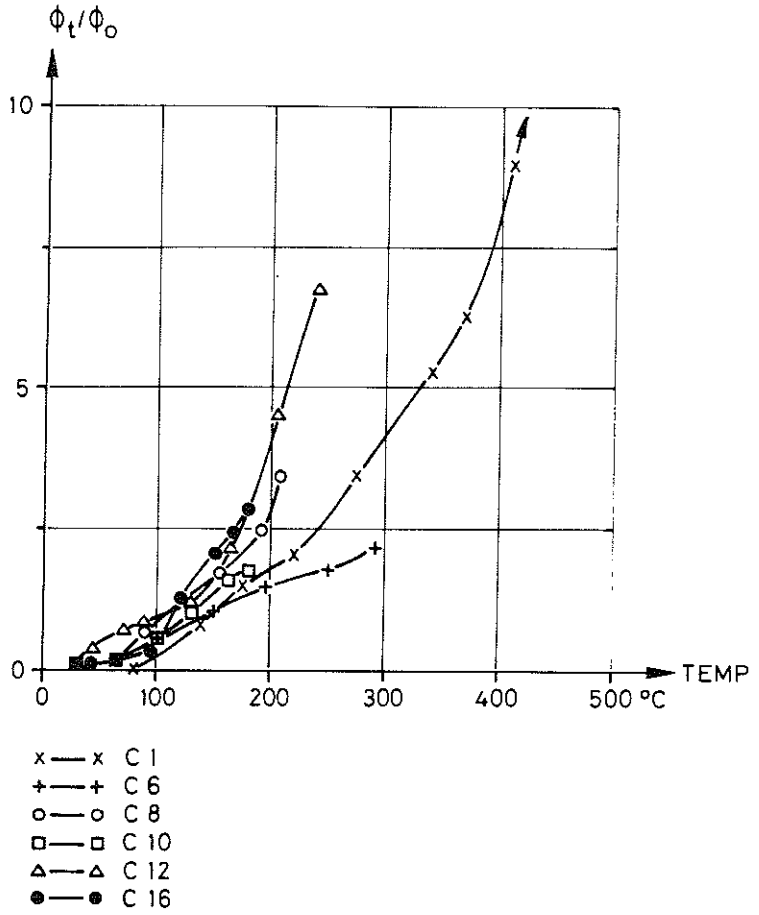

Figure 26. ϕ_t/ϕ_o for six tests in series C as a function of the temperature at a distance 0.7 R_o from the centre of the specimen.
ϕ_t = transient deformation.
ϕ_o = the instantaneous elastic deformation measured for each individual specimen when loaded before heating.

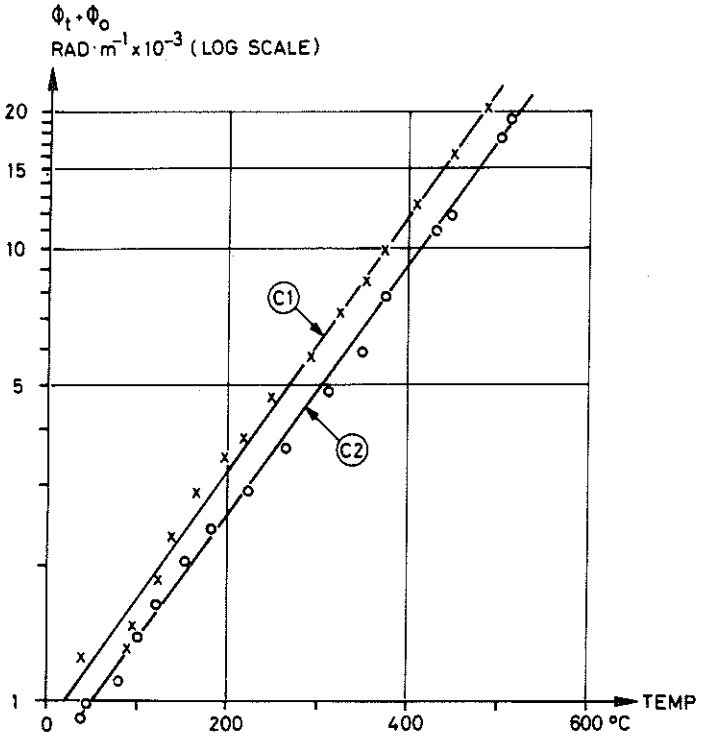

Figure 27. Plot of log ($\phi_t + \phi_o$) against temperature for the tests C1 and C2. The temperature refers to a point at the distance 0.7 R_o from the centre of the specimen. For ϕ_t and ϕ_o see figure 26.

4.3.3 Transient Strain

It will be assumed that the transient strain is time-invariant, thus J_t being a function of temperature only, c.f. 3.4. This component can not be directly measured in tests, since the other strain components will always occur simultaneously. The transient strain is therefore obtained as that part of the total strain, measured under transient conditions, that can not be accounted for otherwise.

It is assumed that the temperature at the distance 0.7 R_o from the centre is representative for the cross section, as was discussed in 3.4 and that eq. (4.8) can be used despite the fact that the temperature is non-uniform over the cross section. Under these assumptions the elastic and the constant temperature creep compliances can be calculated according to eq. (4.11) and (4.16) respectively, and the corresponding values of ϕ_e and ϕ_c are obtained from eq. (4.8). The transient deformation ϕ_t is then obtained by subtracting ϕ_e and ϕ_c from the measured total deformation.

The relation between the different components determined in this way is illustrated in figure 25 for test C1. In spite of the approximations introduced it is obvious that the transient component ϕ_t constitutes the major part of the total deformation. In figure 26 the ratio between the transient deformation ϕ_t and the instantaneous elastic deformation before heating ϕ_o is plotted against temperature for six tests with different loading levels and rates of heating. In view of the approximations inherent in the estimate of ϕ_t the curves are rather near to each other. It should also be noted that yielding immediately before failure is included (see 4.5), which may explain some of the scatter.

To obtain an expression for the transient strain the results from the tests C1 and C2 were used. These tests cover a wider temperature range and the low rate of heating makes it less likely that irregularities due to high thermal gradients are included.

An exponential expression fits well with the data from those tests:

$$J_t = J_o \left(e^{\kappa \cdot (\theta - \theta_o)} - 1\right) \qquad (4.17)$$

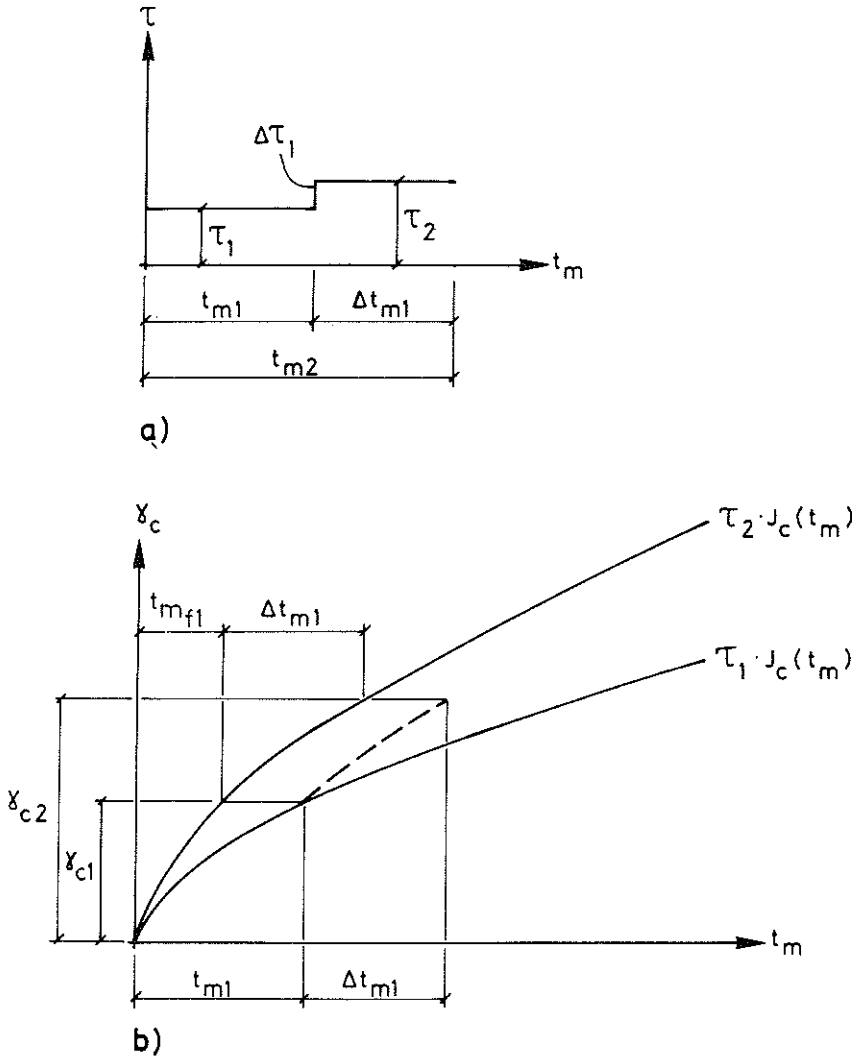

Figure 28. a) Idealized stress variation used to illustrate different superposition principles.

b) The principle of strain hardening applied for the stress variation in a). The full line curves show the creep strain γ_c vs. material time t_m for two different stress levels, τ_1 and τ_2.

where

θ = temperature, ^{o}C

θ_o = initial temperature, ^{o}C

κ = constant, $^{o}C^{-1}$

By plotting log $(\phi_t + \phi_o)$ against θ for the tests C1 and C2 (figure 27) κ can be determined from the slope of the straight lines obtained. The curves are slightly displaced relative to each other due to the different values of ϕ_o (1.24 and $0.88 \cdot 10^{-3}$ rad$\cdot$m^{-1} respectively). The value of κ was in both cases equal to $6.4 \cdot 10^{-3}$ $^{o}C^{-1}$, which value was used in the calculations. The value of θ_o is selected to 20^{o}C.

4.4 Variable Stress

Under constant stress ($\frac{\partial \tau}{\partial t} = 0$) the constitutive equation can be evaluated from the equations (4.6), (4.9), (4.11), (4.16) and (4.17). If the stress varies with the time, which is normally the case, the expressions have to be modified.

As regards the elastic component no problems arise and we can write

$$\gamma_e = \tau \cdot J_e \qquad (4.18)$$

where γ_e = elastic strain component.

For the constant temperature creep component γ_c the question of superposition is far more complicated. In equation (4.16) the compliance J_c is given as a unique function $J_c(t_m)$ of the specific material time t_m, which includes in itself the influence of the temperature history. To illustrate the procedure under variable stress, let us consider a simple case where the stress is varying in two discrete steps as shown in figure 28a. For the first time interval $0 \leq t_m \leq t_{m1}$ the stress has the constant value τ_1 and the strain γ_{c1} at the time t_{m1} will be $\gamma_{c1} = \tau_1 \cdot J_c(t_{m1})$. Proceeding further we want to calculate the strain at the material time $t_{m2} = t_{m1} + \Delta t_{m1}$, and this can be done according to different principles.

One commonly used approach is Boltzmann's superposition principle, which means that every stress increment (positive or negative) should be multiplied by the compliance attained after a time equal to the

duration of the stress increment in question. The algebraic sum of the contributions from all stress changes constitutes the total creep strain. In our case we have

$$\gamma_{c2} = \tau_1 \cdot J_c\,(t_{m2}) + \Delta\tau_1\, J_c\,(\Delta t_{m1}) \qquad (4.19)$$

The Boltzmann superposition principle postulates that γ_c is entirely reversible, which is far from satisfied, cf. 3.5. The application of this principle also leads to complex mathematics, which is hardly justified in this connection.

Another principle is based on the assumption that the material is time hardening. In our case this principle gives

$$\gamma_{c2} = \gamma_{c1} + \tau_2 \cdot \Delta J_{c1} \qquad (4.20)$$

where $\Delta J_{c1} = J_c\,(t_{m2}) - J_c\,(t_{m1})$

This means that the strain increment for a certain time interval is proportional to the actual change in compliance and the actual stress. The strains are assumed to be fully irreversible. This principle is simple to apply but the assumption of time hardening is unrealistic under the actual circumstances.

Therefore, a third method will be used herein, the principle of strain hardening, which can be characterized as a compromise between the two first methods. The creep rate at any instant depends on the actual stress and the accumulated creep strain. In our example we have

$$\gamma_{c2} = \tau_2 \cdot J_c\,(t_{mf1} + \Delta t_{m1}) \qquad (4.21a)$$

where t_{mf1} is a fictitious material time defined by

$$\tau_2 \cdot J_c(t_{mf1}) = \gamma_{c1} = \tau_1 \cdot J_c(t_{m1}) \qquad (4.21b)$$

The principle is illustrated in figure 28b. The strains are fully irreversible - if the stress is removed no further change in γ_c will occur.

Eq. (4.21) is easily generalised to a stress history consisting of an arbitrary number of stress increments and the principle is conveniently adapted to the numerical analysis.

The transient strain component is independent of time and the superposition is therefore not complicated.

When accepting that the transient strain is linear with the stress for constant stress, c.f. eq. (4.6), the only logical way of dealing with variable stress is to assume that the momentary increase of the transient strain γ_t is proportional to the actual stress. This gives

$$\frac{d\gamma_t}{dt} = \tau \cdot \frac{dJ_t}{dt} = \tau \cdot J_o \cdot \kappa \cdot e^{\kappa(\theta-\theta_o)} \cdot \frac{d\theta}{dt} \qquad (4.22)$$

where J_t is taken from eq. (4.17).

Eq. (4.22) illustrates the characteristic features of the transient strain, i.e. that no increase in γ_t will occur if the stress is zero or if the temperature is constant.

The accumulated value of γ_t at the time t for variable stress is given by

$$\gamma_t = \kappa \cdot J_o \cdot \int_0^t \tau \cdot e^{\kappa(\theta-\theta_o)} \cdot \frac{d\theta}{dt} \cdot dt \qquad (4.23)$$

4.5 Failure Criterion

The ultimate stress, which constitutes an upper limit for the stress in each point of the concrete, is continuously varying with the temperature. This variation can be estimated from the data given in figure 13, showing the ultimate torque as a function of temperature. This estimate is difficult to make due to the large scatter in figure 13 and it should be noted that the relation between ultimate torque and stress may depend on the temperature level. However, since the main purpose with the present analysis is not to predict failure but to analyse the deformation behaviour, a rough estimate can be accepted. The temperature dependence is formulated with the following expression:

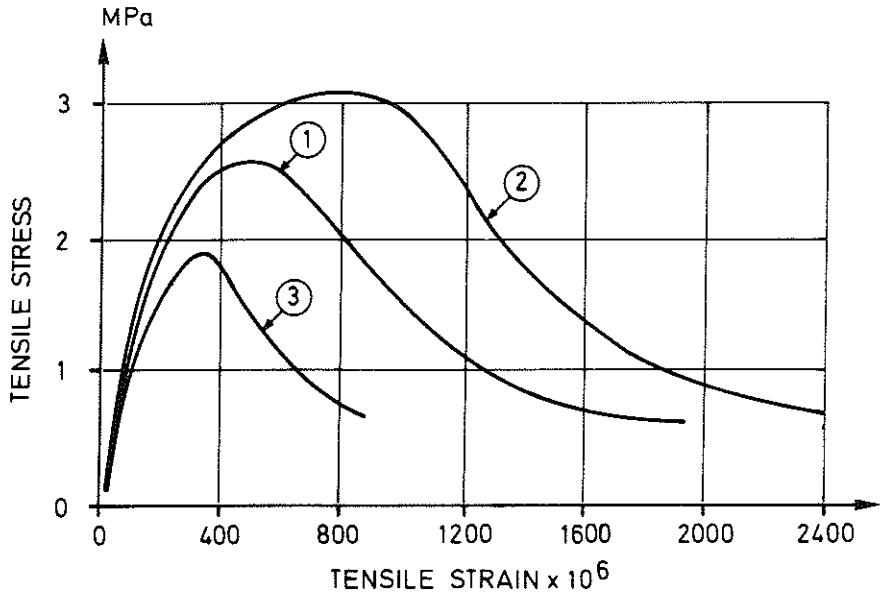

Figure 29. Complete stress strain curves in direct tension from tests with controlled deformation.

Curve	Mix	w/c	Age
1	1:1:2	0.45	65 days
2	1:2:4	0.60	270 days
3	1:3:6	0.90	70 days

$$\tau_u = \tau_{uo} \cdot \exp\left[-2 \cdot 10^{-3} (\theta - 20)\right] \qquad (4.24)$$

where τ_{uo} = the ultimate stress at $20^{\circ}C$.

Eq. (4.24) is shown graphically in figure 13 (curve 3). τ_{uo} is determined from the tests at $20^{\circ}C$ on circular specimens (A1, A3 and A5), where the elastic theory is assumed tc give an acceptable measure on the ultimate stress, cf. 3.1. The ratio between τ_{uo} and the splitting tensile strength at $20^{\circ}C$, σ_{spo} for the tests A1, A3 and A5 is 0.77, 0,77 and 0.76 respectively and τ_{uo} is therefore obtained by

$$\tau_{uo} = 0.77 \cdot \sigma_{spo} \qquad (4.25)$$

where σ_{spo} is the splitting tensile strength determined for the test under consideration.

Now the question is: What happens when the actual stress becomes equal to the ultimate stress in some point (or element)? If the material were perfectly brittle this would imply immediate failure of the specimen. But this is not the case; the material should rather be regarded as elasto-plastic with limited ultimate strain, as it has been shown /24, 25/ that the brittle type of failure, often experienced for concrete in direct tension and also obtained in the torque-twist tests reported herein (figure 15), is primarily caused by the excess energy stored in the testing apparatus. If the tests are performed in a more realistic way, the stress-strain curve in tension has a similar shape as in compression, as shown in figure 29, /25/.

It is assumed here that the material behaves in a perfectly plastic way when the ultimate stress has been reached. Even though it is apparent that the deformability is limited no attempt will be made to estimate any ultimate strain. It is interesting to note in figure 29, however, that an instantaneous non-elastic strain more than three times larger than the elastic strain can develop without any substantial decrease in stress. At higher temperatures the deformability is probably still higher.

The assumption of perfectly plastic behaviour implies that the spe-

cimen fails when the ultimate stress has been attained in all points of the cross section. Whether this state can actually be reached or not under different conditions is uncertain and will be further discussed in connection with the presentation of the results from the theoretical analysis, see 4.7.

The influence of the thermal stresses occuring under transient conditions has been neglected in the above discussion. This is a considerable simplification, since the presence of thermal stresses in one way or another affects the principal stresses, the magnitude of which may be decisive for the occurrence of failure. On the other hand, the plastic behaviour of the material makes it likely that the influence of thermal stresses is small in the ultimate state.

4.6 Method of Calculation

The temperature fields are calculated according to the principles described in 2.5 and the computer program used for this is included as a subroutine in the main program. The temperature is therefore treated as a known quantity in all points at all times.

As mentioned in 4.1 the circular cross section is divided into n ring-shaped elements with a thickness Δr_i and with an average radius r_i. For the sake of clarity the index i will be omitted in what follows and Δr and r as well as the quantities τ, τ_u, γ, t_{mf}, Δt_m, θ, J, Q, P and ξ will always refer to element no i. Summations designated $\sum_n$ refer to the sum of the n ring-shaped elements. The calculation is made stepwise with regard to time and it is assumed that the calculation has proceeded until a certain time t_k. At this time we know the torque $M_{t,k}$, the angle of twist per unit length ϕ_k as well as for each element i the stress τ_k, the strain γ_k, the temperature θ_k, and the fictitious material time $t_{mf,k}$. The equilibrium, compatibility and constitutive equations will be written in incremental form, i.e. in terms of the changes developed during a time step Δt_k. At $t_{k+1} = t_k + \Delta t_k$ we know the temperature θ_{k+1} and we can easily calculate the increment of the specific material time $\Delta t_{m,k}$. In this case we also know the external torsional moment $M_{t,k+1} = M_{t,k} + \Delta M_{t,k}$, whereas the unknown quantities $\phi_{k+1} = \phi_k + \Delta\phi_k$, $\tau_{k+1} = \tau_k + \Delta\tau_k$, and $\gamma_{k+1} = \gamma_k + \Delta\gamma_k$ are to be calculated.

The equilibrium equation (4.2) in incremental form is

$$\Delta M_{t,k} = 2\pi \cdot \sum_{n} \Delta\tau_k \cdot r^2 \cdot \Delta r \qquad (4.26)$$

and the compatibility equation (4.4) is

$$\Delta\gamma_k = r \cdot \Delta\phi_k \qquad (4.27)$$

and the constitutive equation is obtained by

$$\Delta\gamma_k = \Delta\gamma_{e,k} + \Delta\gamma_{c,k} + \Delta\gamma_{t,k} \qquad (4.28)$$

where the indices e, c and t refer to the elastic, constant temperature creep and transient components respectively. The elastic part is obtained by differentiating eq. (4.18):

$$\Delta\gamma_{e,k} = \tau_k \cdot \Delta J_{e,k} + \Delta\tau_k \cdot J_{e,k+1} \qquad (4.29)$$

where

$$\Delta J_{e,k} = J_e(\theta_{k+1}) - J_e(\theta_k)$$

$$J_{e,k+1} = J_e(\theta_{k+1})$$

The function $J_e(\theta)$ is given by eq. (4.11).

To determine the increment of constant temperature creep $\Delta\gamma_{c,k}$, the fictitious material time $t_{mf,k}$ at the beginning of the time step is calculated on the basis of the accumulated creep strain $\gamma_{c,k}$ and the current stress τ_k. The value of $t_{mf,k}$ is given by the following relation

$$\tau_k \cdot J_c(t_{mf,k}) = \gamma_{c,k} \qquad (4.30)$$

with the function $J_c(t_{mf})$ defined by eq. (4.16).

The actual increment of material time $\Delta t_{m,k}$ during the time step Δt_k is obtained by differentiation of eq. (4.15):

$$\Delta t_{m,k} = \exp\left[-\frac{1}{p} \cdot \frac{\Delta H}{R} \left(\frac{1}{T_k + \frac{1}{2}\Delta T_k} - \frac{1}{T_{ref}} \right) \right] \cdot \Delta t_k \qquad (4.31)$$

where

$$T_k = 273 + \theta_k, \text{ K}$$

$$\Delta T_k = \Delta\theta_k, \text{ K}$$

The increment $\Delta J_{c,k}$ of the constant temperature creep compliance is now given by

$$\Delta J_{c,k} = J_c(t_{mf,k} + \Delta t_{m,k}) - J_c(t_{mf,k}) \qquad (4.32)$$

and the increment in creep strain is

$$\Delta\gamma_{c,k} = (\tau_k + \frac{1}{2}\Delta\tau_k)\cdot\Delta J_{c,k} \qquad (4.33)$$

If the stress changes sign, which for instance can happen when the external torsional moment is removed, eq. (4.30) is no longer valid. In this case $t_{mf,k}$ is chosen to zero, i.e. the creep in the reversed direction starts from the beginning on the virgin curve. The case when the sign is changed a second time is beyond the scope of the present investigation and is therefore not considered.

Using the simplest form of numerical integration the transient component $\Delta\gamma_{t,k}$ is obtained from eq. (4.22):

$$\Delta\gamma_{t,k} = J_o\cdot\ \frac{1}{2}\left[\tau_k\cdot\psi_k + (\tau_k + \Delta\tau_k)\cdot\psi_{k+1}\right]\kappa\cdot\Delta\theta_k \qquad (4.34)$$

where

$$\psi_k = \exp\left[\kappa\cdot(\theta_k - \theta_o)\right]$$

$$\psi_{k+1} = \exp\left[\kappa\cdot(\theta_{k+1} - \theta_o)\right]$$

Combining equations (4.28), (4.29), (4.33) and (4.34) yields the complete constitutive equation in incremental form. The constitutive equation so obtained is valid only if the new stress τ_{k+1} does not reach the ultimate limit. The stress increment obtained under this postulate is denoted $\Delta\tilde{\tau}_k$ and is obtained by combining eq. (4.27) with (4.28), (4.29), (4.33) and (4.34):

$$\Delta\tilde{\tau}_k = \frac{r\cdot\Delta\phi_k - \tau_k\cdot Q_k}{P_k} \tag{4.35}$$

where

$$Q_k = \Delta J_{e,k} + \Delta J_{c,k} + J_o\cdot\kappa\cdot\Delta\theta_k\cdot\frac{1}{2}(\psi_k + \psi_{k+1})$$

$$P_k = J_{e,k+1} + \frac{1}{2}\Delta J_{c,k} + J_o\cdot\kappa\cdot\Delta\theta_k\cdot\frac{1}{2}\cdot\psi_{k+1}$$

(For ΔJ_e and ΔJ_c, see eqs. (4.29) and (4.32).

To take into account the case when yielding occurs, i.e. when the stress equals the ultimate limit, a function ξ is defined as follows:

$$\xi_k = \begin{cases} 1 \text{ if } \Delta\tilde{\tau}_k < \tau_{u,k+1} - \tau_k \\ \\ 0 \text{ if } \Delta\tilde{\tau}_k \geq \tau_{u,k+1} - \tau_k \end{cases} \tag{4.36}$$

where $\tau_{u,k+1}$ = ultimate stress in element i at time t_{k+1}.

Accordingly, ξ_k is equal to 1 if yielding does not occur and 0 if yielding occurs.

The actual stress increments $\Delta\tau_k$ is then obtained by:

$$\Delta\tau_k = \xi_k\cdot\Delta\tilde{\tau}_k + (1 - \xi_k)\cdot\left[\tau_{u,k+1} - \tau_k\right] \tag{4.37}$$

If eq. (4.37) is inserted into eq. (4.26) $\Delta\phi_k$ can be obtained explicitly and hence $\Delta\tau_k$ and $\Delta\gamma_k$ are given by the eqs. (4.37) and (4.27) respectively. Thus all unknown quantities at $t = t_{k+1}$ can be determined.

This is possible only if the coefficients ξ_k are known. However, ξ_k can not be evaluated in advance since they depend on $\Delta\tilde{\tau}_k$, which in turn depends on $\Delta\phi_k$. Therefore, as a first approximation it is assumed that $\xi_k = \xi_{k-1}$, that is to say the ξ-values from the previous time step are used. After the calculations for the current time step have been carried out a new set of ξ_k is obtained and it is checked whether these new values are different from the initially assumed ones. If so, the calculation is repeated with the new values until a

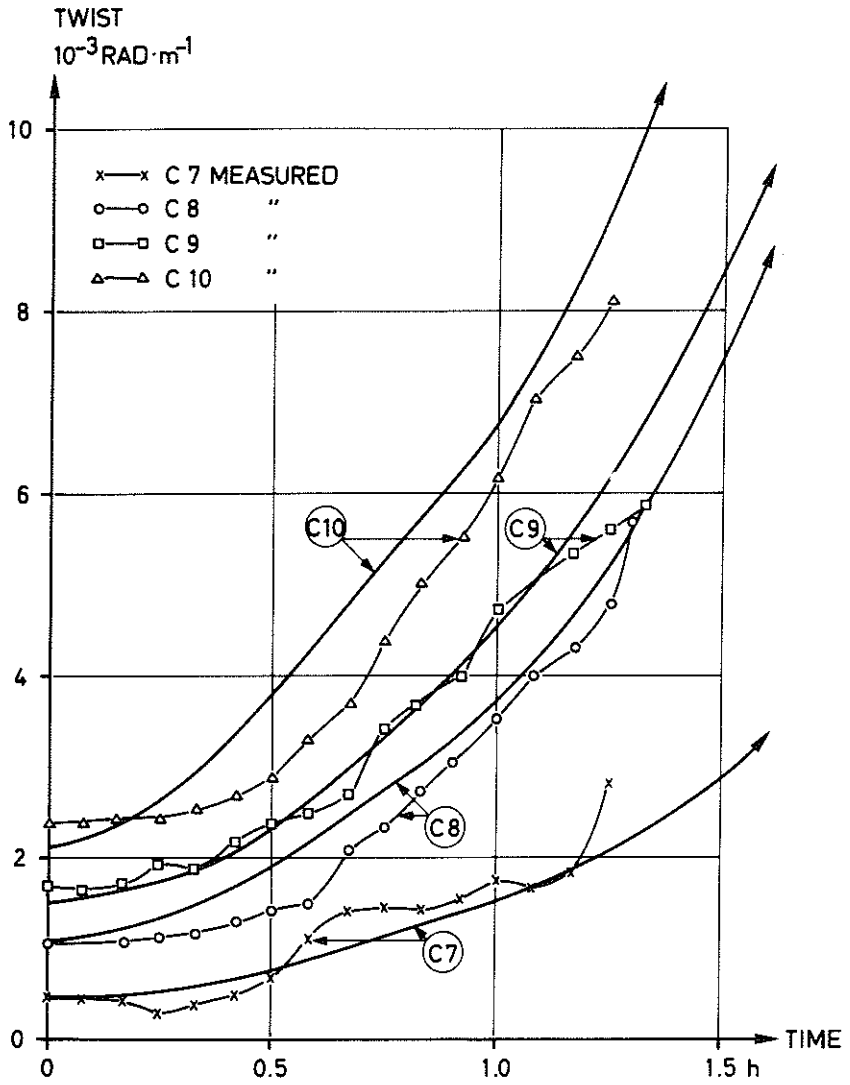

Figure 30. Theoretical and experimental twist-time curves.

TEST	LOAD	$^{o}C \cdot min^{-1}$	G_o (MPa)
C7	15 %	4	15300
C8	30 %	4	11700
C9	45 %	4	13700
C10	60 %	4	12100

consistent solution is obtained.

To avoid convergence problems the conditions in eq. (4.36) were modified to give a certain stability against changes in the ξ-values:

$$\xi_k = \begin{cases} 1 \text{ if } \dfrac{\Delta\tilde{\tau}_k + \tau_k}{\tau_{u,k+1}} < 0{,}99 + 0{,}02 \cdot \xi_{k-1} \\ \text{else } 0 \end{cases} \qquad (4.40)$$

In all calculations performed, seven ring-shaped elements were used. The element placed in the centre of the cross section had a thickness of 15 mm and the other six a thickness of 10 mm each. No significant change in the results was observed when the number of elements were doubled.

4.7 Results from the Calculations

The theory was used to calculate stresses and angular deformations for all the tests from series C and D. In figures 30 and 31 as well as figures A1 - A5 in appendix A, theoretical and experimental twist vs. time curves are compared for the said tests. The input value of the shear modulus at ambient temperature, G_o, which is an important parameter in the calculations, was determined in each individual test on the basis of the deformations upon initial loading. In this way some of the variation in material properties between the individual specimens could be eliminated.

For the tests from series C, figures 30 and A1 - A3,where the specimens were heated to failure, the agreement between theoretical and experimental deformations is extraordinarily good. This is valid for all combinations of load level and rate of heating and, accordingly, the behaviour of individual specimens as illustrated in figures 22 and 26 is correctly predicted by the theory.

Good agreement was also found for the tests of series D shown in figures 31 and A4 - A5, though in some cases the theory gives too small deformations. The latter is particularly the case for the tests D4, D5 and D6, where the specimens were heated to 200°C. As mentioned in 3.4 the results from these particular tests were difficult to interprete, probably due to unstable moisture conditions. It was

also noted that the deformation upon initial loading was virtually independent of the load level, unlike all other tests. But the tendency to underestimate the deformations in series D may also be an effect of the assumption that the transient strain is quasi-instantaneous. A delayed response, if any, to a certain temperature increase is in the present theory implicitly included in subsequent temperature increments and if the temperature increase stops, the deformations may be somewhat underestimated. But in spite of these inevitable uncertanties the theory must be regarded as fully reliable for the prediction of deformations under transient as well as steady state conditions. This is also applicable to the deformation behaviour during and after removal of the external load (figures 31 and A4 - A5).

As regards the prediction of failure, which is applicable to the tests in series C, the picture is somewhat different. In table 2, the predicted and experimentally found times for failure are compared for the 12 tests from series C being analysed. The theoretical value was taken as the time at the beginning of that time step when failure occurred. The predicted failure agrees fairly well with the experimental one for the specimens heated at $2^{\circ}C \cdot min^{-1}$ (tests C1, C2, C5 and C6). In these cases the ultimate stress limit is obviously attained in the whole cross section before failure. For the tests heated at the higher rates $4^{\circ}C \cdot min^{-1}$ and $8^{\circ}C \cdot min^{-1}$ the failure as a rule occurred long before the time predicted in the theory. This is not surprising, since for specimens without load explosive spalling occurred upon heating with the rates 4 and $8^{\circ}C \cdot min^{-1}$ respectively, see 2.5, figures 12b and c. Explosive spalling also occurred in the tests C7 and C8, where the loads applied were comparatively small. Though direct spalling was not observed in the other tests of this category (C9 - C12, C15 - C16), it is probable that high steam pressure in combination with shear stresses and, possibly, thermal stresses has caused the failure. Except for the tests C15 and C16, this failure happens much earlier than the plastic type of failure predicted in the theory and is therefore decisive. We may only conclude that the time of failure predicted in the theory constitutes an upper limit for the capacity of the concrete cross section.

The calculated shear stress distributions obtained for some of the

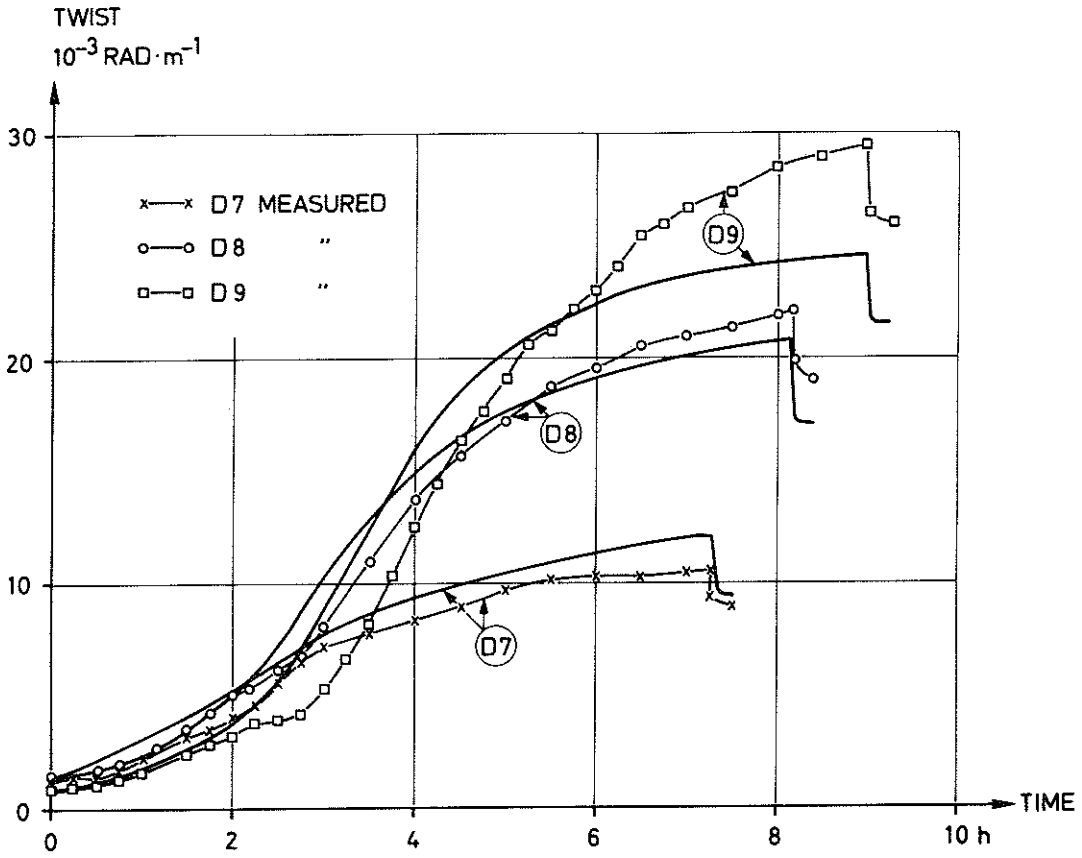

Figure 31. Theoretical and experimental twist-time curves. θ_{max} = = measured maximum temperature near the centre.

TEST	LOAD	θ_{max}	G_o(MPa)
D7	30 %	310	11200
D8	30 %	385	10000
D9	30 %	485	16000

TABLE 2. Theoretical and experimental times of failure for the tests in series C.

Test	Load %	Rate of heating $^{o}C \cdot min^{-1}$	Time of failure Theory min	Exp min
C1	30	2	315	296
C2	30	2	309	310
C5	60	2	180	167
C6	60	2	177	154
C7	15	4	>192[1]	75[2]
C8	30	4	>162[1]	78[2]
C9	45	4	156	80
C10	60	4	123	75
C11	30	8	117	54
C12	30	8	111	59
C15	60	8	57	56
C16	60	8	54	52

1) The calculation was terminated prior to theoretical failure

2) The specimens failed in explosive spalling

tests are shown in figures A6 - A8 at selected times after the start of heating. The stresses immediately before theoretical failure are also shown where it is appropriate. The initially linear distribution of stress changes upon heating in such a way that the stresses in the regions with high temperature (near the surface) are relieved and the point of maximum stress moves inwards. The redistribution of stresses is more marked at higher rates of heating when the thermal gradients are steeper. The most dramatic redistributions occur immediately after the experimental failure and are thus purely theoretical (tests C8, C12 and C10). In such cases very high shear stresses are found in the central part of the specimen where the steam pressure is high and where tensile stresses due to thermal gradients may develop, which can explain the early failure.

In figure A8 are shown the calculated stresses for test D8, in which test the temperature was stabilized at about 400°C. In the early stages the stress distribution is similar to that in figure A6, but when the temperatures become uniform ($t \geq 240$ min) over the cross section the stress distribution becomes again approximately linear. When the load is removed only small residual stresses are left.

5. Concluding Remarks

The deformations occurring in loaded concrete under transient temperature conditions can not be predicted only from data obtained at steady state conditions. The deformation under load is much greater during heating than at constant temperature. This applies to the first heating - for subsequent cycles the behaviour is different.

A constitutive equation which adequately describes the deformation behaviour in torsion under non-steady conditions can be formulated in terms of the following three strain components

Elastic strain
Constant temperature creep strain
Transient strain.

The elastic strain is determined by the shear modulus, which is a function of temperature. The constant temperature creep is the time dependent strain measured under constant stress and temperature, whereas the transient strain component occurs only if the temperature increases in the concrete under load. The transient strain is a new concept introduced on a purely phenomenological basis and there is nothing corresponding to it in classical rheology.

It may be interesting to consider the possibility of describing the actual behaviour of heated, loaded concrete on the basis of a conventional creep theory. A way to do it might be to see the sum of the transient strain and the constant temperature creep as time-dependent creep obeying the time-hardening principle of superposition. The rapid response to temperature increase exhibited by the concrete might then be taken into account in the choice of time and temperature functions. But this is difficult to accomplish and the necessary creep constants would be hard to determine. The approach used herein is more directly related to the kind of test data that can be obtained.

All three strain components are linearly related to the stress, which gives good agreement between theory and experiments. The model can, however, easily be modified to a non-linear stress dependence when and if this is necessary.

It should be noted that drying creep is implicitly included in the transient strain, since drying and temperature increase occur simultaneously. It remains to be investigated if and how the transient strain is affected by the initial moisture content and other parameters determining the moisture migration. The strain behaviour under cooling has not been considered in this study, but it is likely that the transient strain rate is zero when the temperature decreases as it is under constant temperature. This remains to be fully proved, however.

The constitutive relation can be further simplified if the constant temperature creep component, which constitutes a minor part of the total strain, is included in the elastic strain in one way or another. This can form a basis for very simple methods of analysis being sufficiently accurate for many practical purposes.

The reliability of the theory is proved by the good agreement obtained in the analysis of the torsion tests, which cover a wide range of load and heating conditions. It is believed that the suggested constitutive model in a qualitative sense also can be used to describe the strain behaviour in compression and direct tension, though in these cases the thermal expansion must be taken into account. In a coming paper by the author and Anderberg the strain behaviour in compression will be analysed on the basis of a comprehensive test series involving the same types of tests as those accounted for in this paper, see also /6/.

The practical implication of such studies is that a thorough understanding of the structural behaviour of thermally exposed concrete structures can be gained. This can in turn lead to the development of simplified methods which can be used for design purposes.

References

/1/ Harmathy, T.Z.: Deflection and Failure of Steel-Supported Floors and Beams in Fire. National Research Council, Canada, Division of Building Research, Paper No. 195, Ottawa 1966.

/2/ Thor, J.: Deformations and Critical Loads of Steel Beams under Fire Exposure Conditions. National Swedish Council for Building Research, Document D16:1973, Stockholm 1973.

/3/ Bazant, Z.P.: Constitutive Equation for Concrete Creep and Shrinkage Based on Thermodynamics of Multiphase Systems, Rilem Bulletin V.3, No. 13, Jan.-Febr. 1970, pp 1 - 36.

/4/ Fahmi, H.M., Polivka, M., Bresler, B.: Effect of Sustained and Cyclic Elevated Temperatures on Creep of Concrete. Cement and Concrete Research, V.2. No. 5, Sept 1972, pp 591 - 606.

/5/ Fahmi, H.M., Bresler, B., Polivka, M.: Prediction of Creep of Concrete at Variable Temperatures. ACI Journal, Proceedings V.70, Oct. 1973, pp 709 - 713.

/6/ Anderberg, Y., Thelandersson, S.: Deformation Characteristics of Concrete at High Temperatures 1. General Discussion and Critical Review of Literature. Division of Structural Mechanics and Concrete Construction, Lund Institute of Technology, Bulletin No. 34, Lund, Sweden, 1973.

/7/ Hansen, T.C., Eriksson, L.: Temperature Change Effect on Behaviour of Cement Paste, Mortar and Concrete Under Load, ACI Journal, Proceedings V. 63, April 1966, pp 489 - 504.

/8/ Illston, J.M., Sanders, P.D.: The Effect of Temperature Change Upon the Creep of Mortar Under Torsional Loading. Magazine of Concrete Research, Vol. 25, No. 84, Sept. 1973.

/9/ Nishizawa, N., Okamura, H.: Strength and Inelastic Properties of Concrete at Elevated Temperature. Concrete for Nuclear Reactors, ACI SP-34, Detroit 1972.

/10/ Ruetz, W.: Hypothesis for the Creep of Hardened Cement Paste and the Influence of Simultaneous Shrinkage. International Conference on the Structure of Concrete, London, Cement and Concrete Association, pp 365 - 387, 1967.

/11/ Ödeen, K.: Fire Resistance of Prestressed Concrete Double T Units. Acta Polytechnica Scandinavica Ci 48, Stockholm 1968.

/12/ Mukaddam, M.A., Bresler, B.: Behaviour of Concrete Under Variable Temperature and Loading. Concrete for Nuclear Reactors, SP-34, American Concrete Institute, Detroit, 1972, pp 771 - 797.

/13/ Ödeen, K., Nordström, Å.: Termiska egenskaper hos betong vid höga temperaturer. (Thermal Properties of Concrete at High Temperatures). Cement och Betong 1972:1, Stockholm.

/14/ Nekrassow, K.D., Joukov, V.V., Shevchenko, V.I.: Investigation of Heating Large Blocks of Refractory Concrete from One Side. Refractories (Translation from Ogneupory, No. 6, pp 21 - 26, June 1967), New York 1967.

/15/ Thelandersson, S.: Effects of High Temperatures on Tensile Strength of Concrete. Nordisk Betong 1972:2.

/16/ Zoldners, N.G.: Effect of High Temperatures on Concrete Incorporating Different Aggregates. ASTM Proceedings Volume 60, 1960.

/17/ Marshall, W.T., Tembe, N.R.: Experiments on Plain and Reinforced Concrete in Torsion. Structural Engineer, London, V. 19, No. 11, Nov. 1941, pp 177 - 191.

/18/ Hsu, T.T.C.: Torsion of Structural Concrete - Plain Concrete, Rectangular Sections. ACI Special Publication No. 18, Detroit 1968, pp 203 - 238.

/19/ Cruz, C.R.: Elastic Properties of Concrete at High Temperatures. Journal of the PCA Res. and Dev. Lab., Jan. 1966.

/20/ Maréchal, J.C.: Le fluage du béton en fonction de la température. Materials and Structures, RILEM bulletin, No. 2, pp 111 - 115, 1969.

/21/ Ruetz, W.: Das Kriechen des Zementsteins im Beton und seine Beeinflussung durch gleichzeitiges Schwinden. Deutscher Ausschuss für Stahlbeton, Heft 183, Berlin 1966, p. 29.

/22/ Schneider, U.: Zur Kinetik festigkeitsmindernder Reaktionen in Normalbetonen bei hohen Temperaturen. Dissertation, Technische Universität Braunschweig, Dec. 1973, p. 94.

/23/ Pipkin, A.C.: Lectures on Viscoelastic Theory. Applied Mathematical Sciences 7. Springer-Verlag, New York 1972.

/24/ Hughes, B.P., Chapman, G.P.: The Complete Stress-Strain Curve for Concrete in Tension. RILEM bulletin, No, 30, March 1966.

/25/ Evans, R.M., Marathe, M.S.: Microcracking and Stress Strain Curves for Concrete in Tension. RILEM bulletin, No. 1, Jan. - Febr. 1968, pp 61 - 64.

/26/ Becker, J., Bresler, B.: Fires-RC. A Computer Program for the Fire Response of Structures - Reinforced Concrete Frames. University of California, Berkeley, Fire Research Group 74-3, July 1974.

Main Symbols

Latin

G_o	shear modulus at ambient conditions	MPa
G_θ	shear modulus at temperature θ	MPa
ΔH	activation energy for creep	$J \cdot mole^{-1}$
I_p	polar moment of inertia	m^4
i_v	enthalpy	$MJ \cdot m^{-3}$
$J=J(\theta,t)$	compliance	MPa^{-1}
ΔJ	increment of compliance	MPa^{-1}
J_o	elastic compliance at ambient temperature	MPa^{-1}
M_t	torque, torsional moment	$N \cdot m$
M_{tu}	ultimate torque	$N \cdot m$
p	dimensionless coefficient	-
P	expression defined in eq. 4.35	MPa^{-1}
Q	" " " " "	MPa^{-1}
r	coordinate in radial direction	m
R	gas constant	$J \cdot mole^{-1} \cdot K^{-1}$
R_o	radius of circular cross section	m
r_i	radius of ringshaped element no. i	m
Δr_i	thickness of ditto	m
t	time coordinate	s
t_m	specific material time	s
t_{mf}	specific material time, fictitious value	s
Δt_m	increment of specific material time	s
t_{ref}	reference time	s
T	absolute temperature	K
T_{ref}	absolute temperature, reference value	K
ΔT	temperature increment	K

Greek

β	dimensionless coefficient	-
γ	shear strain	Rad
$\Delta\gamma$	increment of shear strain	Rad
θ	temperature	^oC
θ_o	initial temperature	^oC
θ_{ref}	reference temperature	^oC
$\Delta\theta$	temperature increment	^oC

κ	constant	$^{o}C^{-1}$
λ	thermal conductivity	$W \cdot m^{-1} \cdot {}^{o}C^{-1}$
ξ	dimensionless function defined by eq. (4.36)	-
σ_{cube}	cube strength obtained on 150 mm cubes	MPa
σ_{spo}	splitting tensile strength at ambient conditions	MPa
τ	shear stress	MPa
$\Delta\tau$	increment of shear stress	MPa
$\Delta\tilde{\tau}$	increment of shear stress provided that yielding does not occur	MPa
τ_u	ultimate shear stress	MPa
τ_{uo}	ultimate shear stress at ambient conditions	MPa
ϕ	angle of twist per unit length	$Rad \cdot m^{-1}$
ϕ_o	angle of twist at initial loading	$Rad \cdot m^{-1}$
$\Delta\phi$	increment of angular deformation	$Rad \cdot m^{-1}$
ψ	dimensionless expression defined in eq. (4.34)	-

Indices

c	constant temperature creep component
e	elastic component
i	of ringshaped element i
k	at the time t_k
t	transient component

APPENDIX A. RESULTS FROM THE CALCULATIONS.

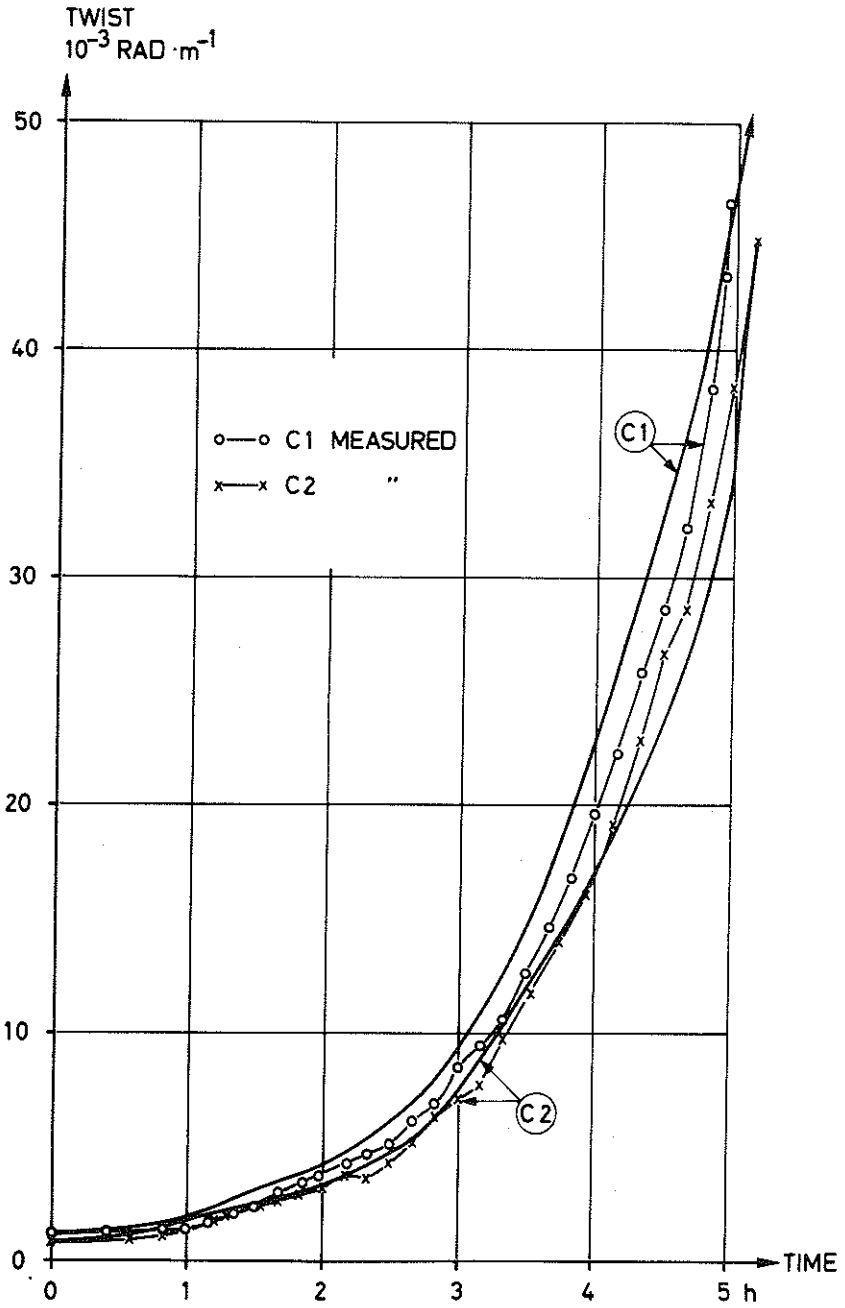

Figure A1. Theoretical and experimental twist-time curves.

TEST	LOAD	$^{o}C \cdot min^{-1}$	G_o(MPa)
C1	30 %	2	10250
C2	30 %	2	14800

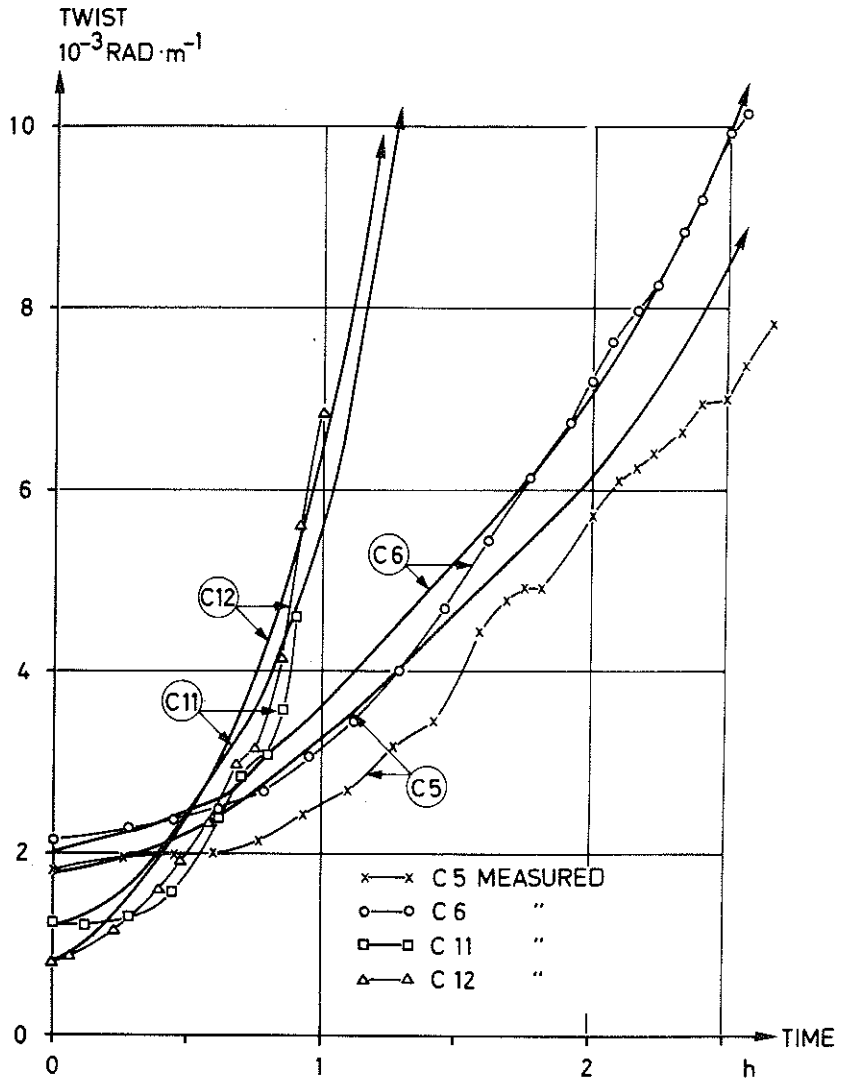

Figure A2. Theoretical and experimental twist-time curves.

TEST	LOAD	$^{o}C \cdot min^{-1}$	G_o (MPa)
C5	60 %	2	14500
C6	60 %	2	13300
C11	30 %	8	12700
C12	30 %	8	16000

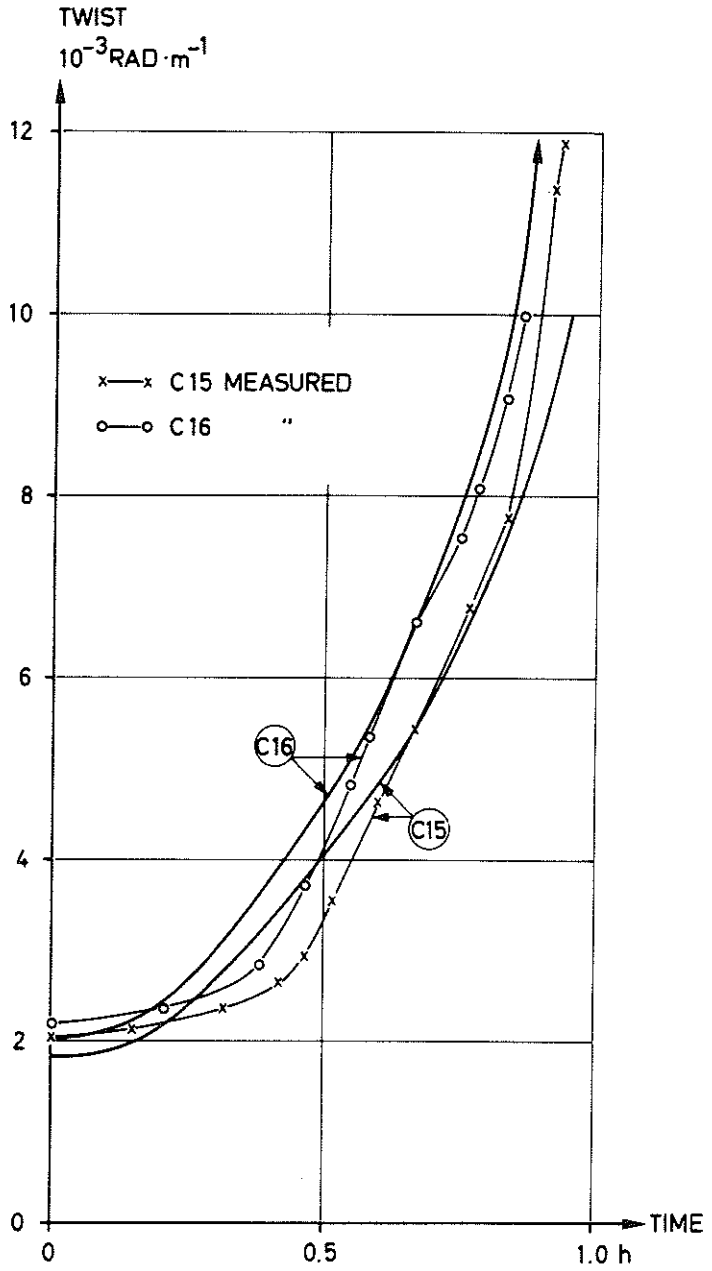

Figure A3. Theoretical and experimental twist-time curves.

TEST	LOAD	$^{o}C \cdot min^{-1}$	G_o(MPa)
C15	60 %	8	13900
C16	60 %	8	12800

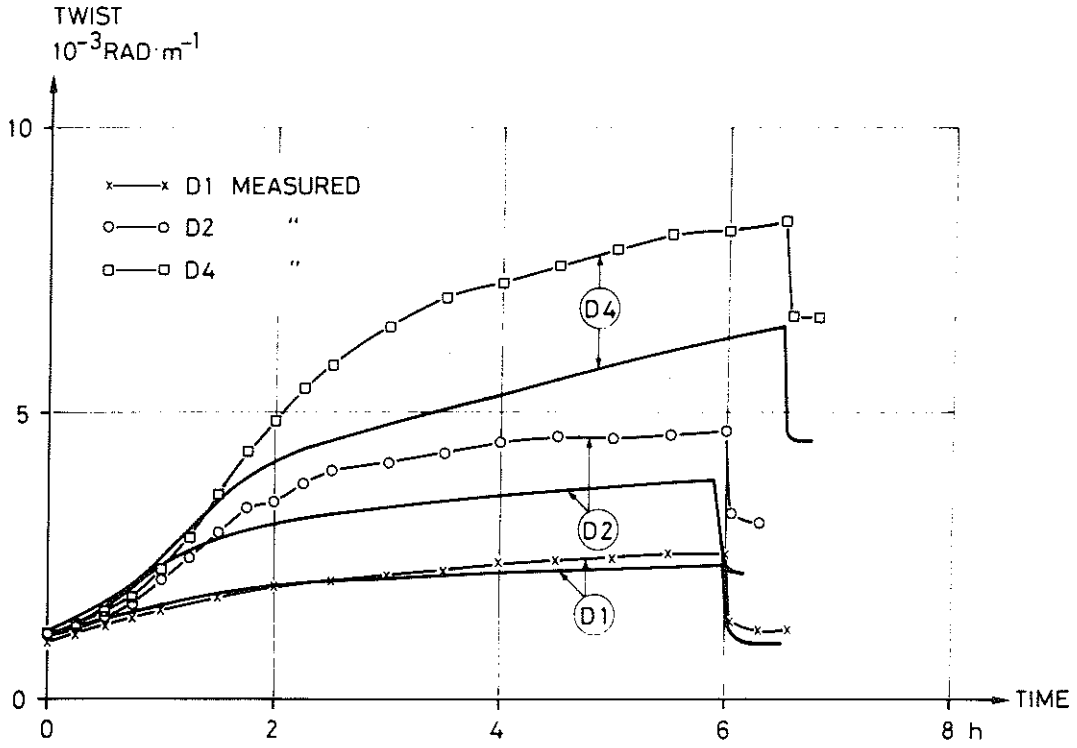

Figure A4. Theoretical and experimental twist-time curves. θ_{max} = = measured maximum temperature near the centre.

TEST	LOAD	θ_{max}	G_o
D1	30 %	80	11800
D2	30 %	135	12100
D4	30 %	205	11100

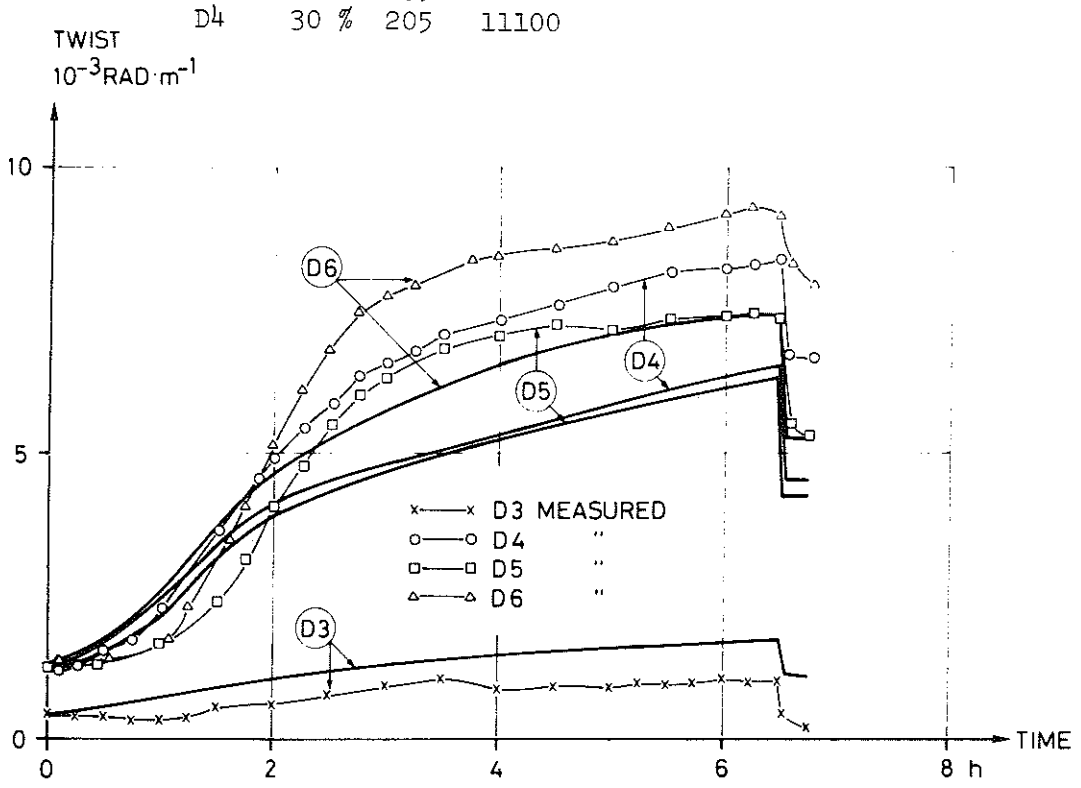

Figure A5. Theoretical and experimental twist-time curves. θ_{max} = = measured maximum temperature near the centre.

TEST	LOAD	θ_{max}	G_o (MPa)
D3	15 %	165	16300
D4	30 %	205	11100
D5	45 %	195	16000
D6	60 %	210	20800

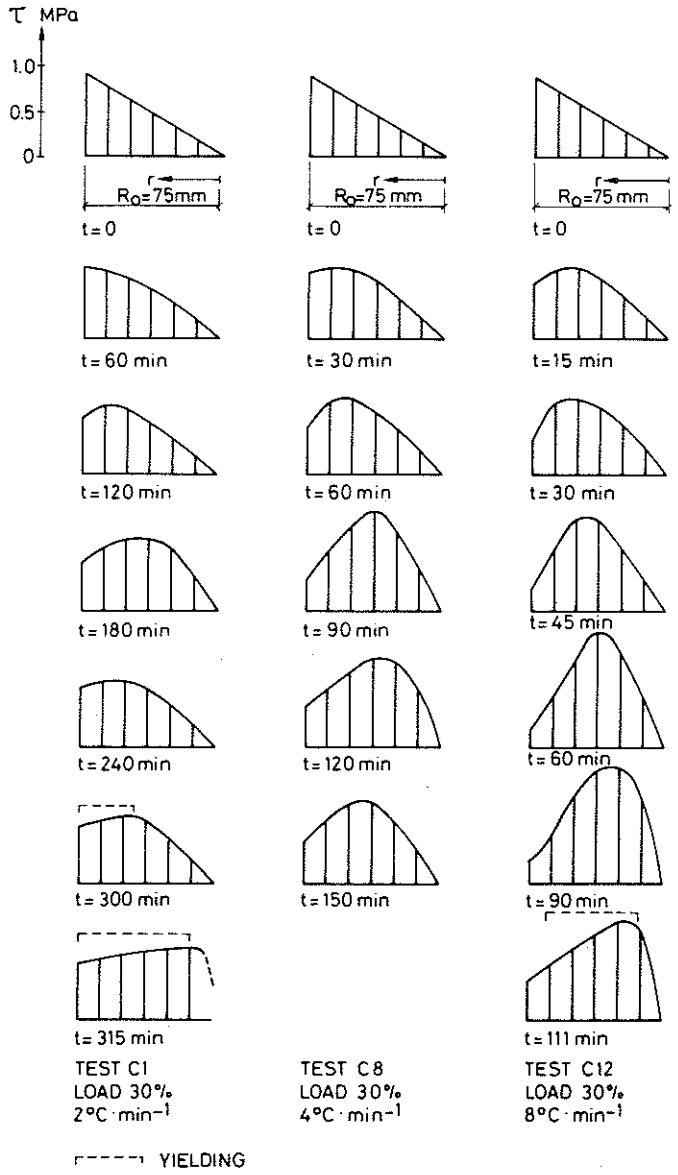

Figure A6. Theoretical shear stress distributions at different times from the start of the tests C1, C8 and C12.
r = distance from the centre of the specimen.
R_o = radius of the circular cross section.

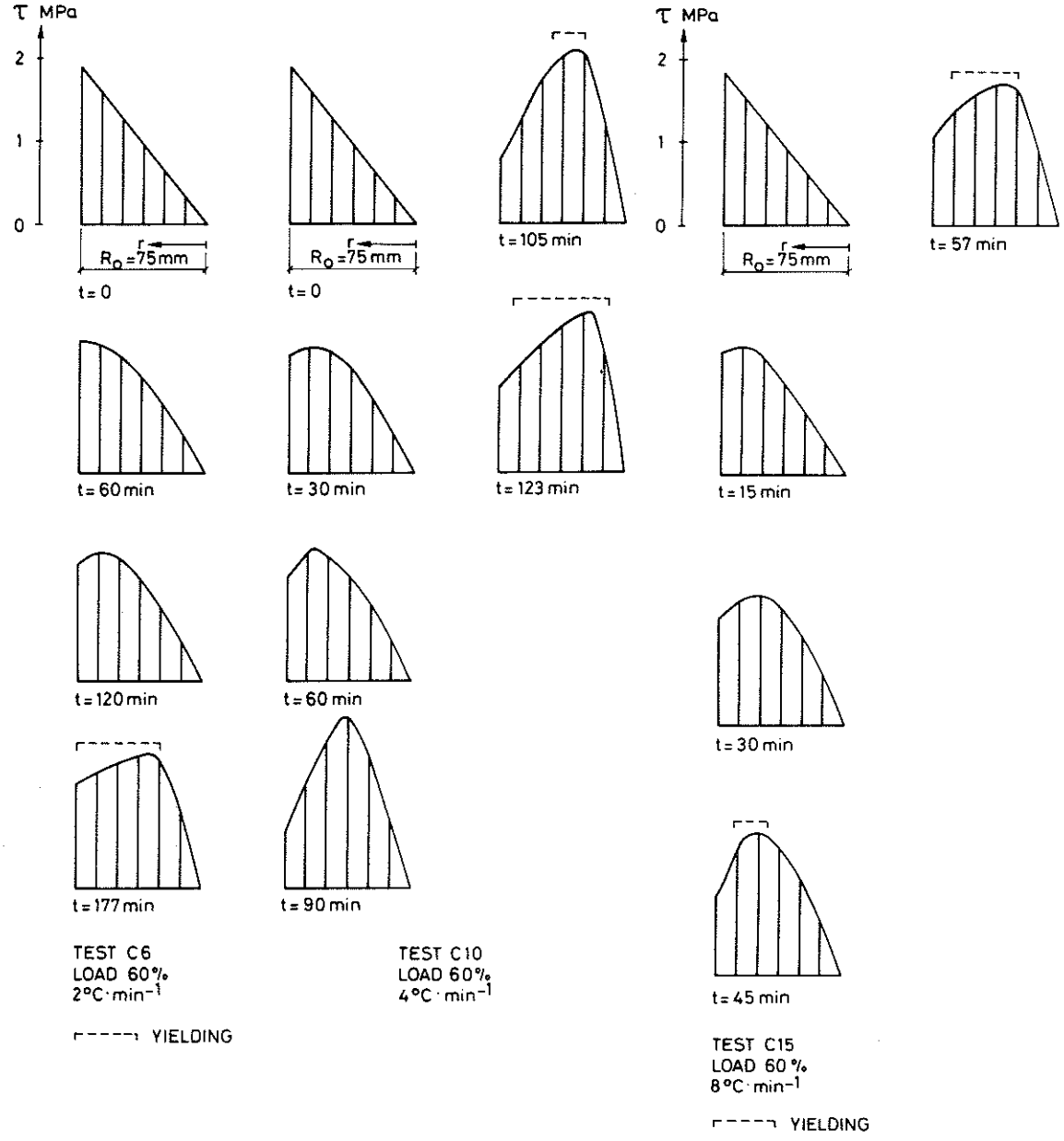

Figure A7. Theoretical shear stress distributions at different times from the start of the tests C6, C10 and C15. For r and R_0 see figure A6.

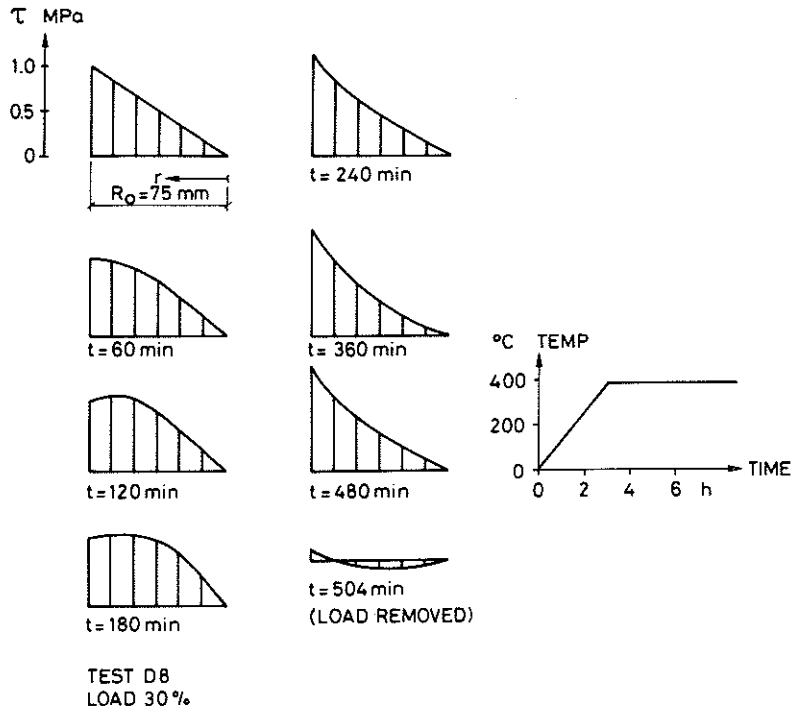

Figure A8. Theoretical shear stress distributions at different times from the start of the test D8. For r and R_o see figure A6. The actual furnace temperature history is shown in the figure.